Genetic evidence for the involvement of mismatch repair proteins, PMS2 and MLH3, in a late step of homologous recombination

Received for publication, March 19, 2020, and in revised form, September 28, 2020 Published, Papers in Press, October 2, 2020, DOI 10.1074/jbc.RA120.013521

Md Maminur Rahman[1,‡], Mohiuddin Mohiuddin[1,‡], Islam Shamima Keka[1], Kousei Yamada[1], Masataka Tsuda[1], Hiroyuki Sasanuma[1], Jessica Andreani[2], Raphael Guerois[2], Valerie Borde[3], Jean-Baptiste Charbonnier[2], and Shunichi Takeda[1,*]

From the [1]Department of Radiation Genetics, Graduate School of Medicine, Kyoto University, Yoshida-Konoe-cho, Kyoto, Japan, the [2]Institute for Integrative Biology of the Cell (I2BC), Commissariat à l'Energie Atomique (CEA), CNRS, Université Paris-Saclay, Gif-sur-Yvette, France, and the [3]Institut Curie, CNRS UMR3244, PSL Research University, Paris, France

Edited by Patrick Sung

Homologous recombination (HR) repairs DNA double-strand breaks using intact homologous sequences as template DNA. Broken DNA and intact homologous sequences form joint molecules (JMs), including Holliday junctions (HJs), as HR intermediates. HJs are resolved to form crossover and noncrossover products. A mismatch repair factor, MLH3 endonuclease, produces the majority of crossovers during meiotic HR, but it remains elusive whether mismatch repair factors promote HR in nonmeiotic cells. We disrupted genes encoding the MLH3 and PMS2 endonucleases in the human B cell line, TK6, generating null *MLH3*$^{-/-}$ and *PMS2*$^{-/-}$ mutant cells. We also inserted point mutations into the endonuclease motif of *MLH3* and *PMS2* genes, generating endonuclease death *MLH3*$^{DN/DN}$ and *PMS2*$^{EK/EK}$ cells. *MLH3*$^{-/-}$ and *MLH3*$^{DN/DN}$ cells showed a very similar phenotype, a 2.5-fold decrease in the frequency of heteroallelic HR-dependent repair of restriction enzyme–induced double-strand breaks. *PMS2*$^{-/-}$ and *PMS2*$^{EK/EK}$ cells showed a phenotype very similar to that of the MLH3 mutants. These data indicate that MLH3 and PMS2 promote HR as an endonuclease. The *MLH3*$^{DN/DN}$ and *PMS2*$^{EK/EK}$ mutations had an additive effect on the heteroallelic HR. *MLH3*$^{DN/DN}$/*PMS2*$^{EK/EK}$ cells showed normal kinetics of γ-irradiation–induced Rad51 foci but a significant delay in the resolution of Rad51 foci and a 3-fold decrease in the number of cisplatin-induced sister chromatid exchanges. The ectopic expression of the Gen1 HJ resolvase partially reversed the defective heteroallelic HR of *MLH3*$^{DN/DN}$/*PMS2*$^{EK/EK}$ cells. Taken together, we propose that MLH3 and PMS2 promote HR as endonucleases, most likely by processing JMs in mammalian somatic cells.

The mismatch repair (MMR) pathway corrects the mismatch formed during DNA replication (1–5). MMR is initiated by the recognition of mismatches by the heterodimers MSH2-MSH6 (MutSα) and MSH2-MSH3 (MutSβ) (5–10). Upon recognition, the MutS heterodimers interact with one of the three MutL heterodimers MLH1-PMS2 (MutLα), MLH1-PMS1 (MutLβ), or MLH1-MLH3 (MutLγ) (11–13). A single-strand break formed by the MLH1-PMS2 endonuclease serves as entry point for the exonuclease activity that removes mismatched DNA. The endonuclease activity of MLH1-PMS2 depends on the metal-binding motif DQHAX_2EX_4E present on PMS2 and the last 10 residues of MLH1 (14). This nuclease-active site is conserved in MLH3 but not in PMS1 (15).

A subclass of the MMR proteins is involved in double-strand break (DSB) repair. First, MutS complexes play a role in the rejection of heteroduplex DNA containing insertion/deletion mismatches when the nucleotide sequences of two partner DNAs are not identical (16, 17). Second, MutSα may recognize mismatches within the heteroduplex region of the JMs and avoid recombination, collaborating with RecQ helicases (18). Third, MLH1 can affect nonhomologous end-joining (NHEJ) (19), which repairs 80% of the ionizing radiation–induced DSB in the G_2 phase (20). Fourth, a subset of MSH and MLH proteins promote meiotic HR, a function distinct from their MMR functions. MLH1-MLH3, which has a minor role in MMR, is critical for producing meiotic crossover products in mice and *Saccharomyces cerevisiae* (21, 22). MLH1, MLH3, and PMS2 are essential for the progression of meiotic HR in mice (23–28). The role played by the putative endonuclease activity of PMS2 in the resolution of meiotic HR intermediates has not yet been clarified in mice or humans, but recent studies have unveiled new insights into the molecular mechanisms of MLH1-MLH3 and the role of its endonuclease activity (22, 29, 30). Another unsolved question is whether MLH3 and PMS2 promote HR in mammalian somatic cells.

HR initiates DSB repair by resecting DSBs, leading to the formation of 3′ single-strand overhangs, followed by polymerization of Rad51 on the single-strand DNA (31–33). The resulting Rad51 nucleoprotein filaments undergo homology search and pairing with the intact duplex DNA donor to form joint molecules (JMs) such as double Holliday junctions (dHJs) with the help of Rad54 (33–35). JMs are resolved into individual DNA duplexes to allow chromosomes to separate in the anaphase.

This article contains supporting information.

‡These authors contributed equally to this work.
*For correspondence: Shunichi Takeda, stakeda@rg.med.kyoto-u.ac.jp.
Present address for Mohiuddin: Program of Genetics and Genome Biology, Hospital for Sick Children, Toronto, Ontario, Canada.
Present address for Islam Shamima Keka: Program of Genetics and Genome Biology, Hospital for Sick Children, Toronto, Ontario, Canada.
Present address for Masataka Tsuda: Program of Mathematical and Life Science, Graduate School of Integrated Sciences for Life, Hiroshima University, Higashi-Hiroshima, Japan.

The separation is performed by two alternative processes, the dissolution and resolution pathways. The phenotypic analysis of meiotic HR indicates that only 10% of the DSBs (*Mus musculus*) form dHJs, and these are almost exclusively processed by the resolution pathway, involving the activity of MLH1-MLH3 (22). In somatic cells, the resolution of HJs is done by a number of structure-specific endonucleases, MUS81-EME1, SLX1-SLX4, XPF-ERCC1, and GEN1 (36–39). Mice deficient in either MUS81-EME1 or SLX1-SLX4 or GEN1 are all viable, whereas mice deficient in both MUS81-EME1 and GEN1 are synthetic lethal (40–43), suggesting a substantial functional overlap between the two nucleases. Although yeast genetic studies have precisely monitored the formation of HR intermediate molecules such as HJs over time upon DSB formation during both meiosis and mitosis (21, 34, 44, 45), no equivalent phenotypic assays are available in the phenotypic analysis of HR in mammalian somatic cells.

There are two major DSB repair pathways in mammalian cells, HR and NHEJ. The two pathways differentially contribute to cellular tolerance to anti-malignant therapies. These pathways contribute to tolerance to radiotherapy with HR functioning in the S to G_2 phases and NHEJ functioning in the whole cell cycle (46). HR, but not NHEJ, repairs DSBs induced by camptothecin (Top1 poison) and olaparib (poly(ADP-ribose) polymerase poison). NHEJ plays the dominant role in repairing DSBs induced by ICRF-193 (catalytic inhibitor of Top2) (47, 48). Thus, the sensitivity profile of DSB-repair mutants to these chemotherapeutic agents helps to discriminate which repair pathway is compromised in the mutants.

To investigate the role for MLH3 and PMS2 as nucleases in DSB repair of somatic mammalian cells, we inserted a point mutation into the DQHAX_2EX_4E motif of the endogenous *MLH3* and *PMS2* genes of the human TK6 B cell line (49) and generated $MLH3^{D1223N/D1223N}$ and $PMS2^{E705K/E705K}$ cells. These mutants exhibited increased sensitivities to camptothecin and olaparib, a few-fold decrease in the frequency of both sister chromatid exchange (SCE) and the heteroallelic HR, and delayed resolution of γ-ray–induced Rad51 foci, indicating a defect in HR in later steps. Surprisingly, their role seems to be mostly independent of MLH1. We conclude that the MLH3 and PMS2 proteins promote DSB repair by HR, presumably by processing JMs in human cells.

Results

MLH3 and PMS2 mutants, but not MSH2 and MLH1 mutants, are sensitive to both camptothecin and olaparib

We disrupted the *PMS2* and *MLH3* genes in TSCER2 cells (50, 51), a TK6 subline for measuring heteroallelic HR, generating $PMS2^{-/-}$ and $MLH3^{-/-}$ cells (Figs. S1 and S2). We also generated $MSH2^{-/-}$ cells (Figs. S3, *A* and *B*), as MSH2 plays a major role in MMR but is not involved in the resolution of HJs in *S. cerevisiae* (21). $MSH2^{-/-}$ cells were tolerant to an alkylating agent, temozolomide (Fig. S3*C*), as expected from a defect in MMR (52). $PMS2^{-/-}$ and $MLH3^{-/-}$ cells were sensitive to camptothecin, γ-irradiation, and olaparib (Fig. 1, *A* and *B*), whereas $MSH2^{-/-}$ cells were tolerant to these damaging agents (Figs. S3, *D–F*). These data suggest the involvement of PMS2 and MLH3 in HR-dependent DSB repair independently of their functioning in MMR or independently of their interaction with MutSα (MSH2-MSH6) or MutSβ (MSH2-MSH3) heterodimers. We generated $MLH1^{-/-}$ cells (Fig. S4, *A–E*) and verified a defect in MMR by confirming the marked tolerance to temozolomide (53) (Fig. S4*F*). We found no noticeable sensitivity of $MLH1^{-/-}$ cells to camptothecin, γ-irradiation, and olaparib (Fig. 1*A*). In addition, we completely deleted the whole *MLH1* locus (57 kb) from TK6 cells (Fig. S4, *G–I*) and confirmed that the resulting *MLH1* null cells were tolerant to camptothecin (Fig. S4*J*). We disrupted the *MUS81* gene in *WT* and $PMS2^{-/-}$ TK6 clones (Fig. S5). The resulting $MUS81^{-/-}$ cells showed a phenotype very similar to that of $PMS2^{-/-}$ cells. $MUS81^{-/-}/PMS2^{-/-}$ cells showed higher sensitivity to olaparib than $MUS81^{-/-}$ and $PMS2^{-/-}$ cells (Fig. 1*C*). These observations support the notion that PMS2 and MUS81 act independently of each other in HR-mediated DSB repair.

To investigate the catalytic role of MLH3 and PMS2, we inserted point mutations into the endogenous *MLH3* and *PMS2* genes at the highly conserved DQHAX_2EX_4E metal-binding motif. The replacement of the glutamic acid residue in position 705 by lysine (E705K) in human PMS2 completely inactivates its endonuclease activity (15, 54, 55). Likewise, the D523N and E529K mutations in *S. cerevisiae* MLH3, which correspond to the D1223N and E1229K mutations in human MLH3, impair both MMR and the resolution of JMs in meiotic HR in mice and *S. cerevisiae* (21, 22, 29, 56–58). We thus generated $PMS2^{E705K/E705K}$ cells (Fig. S1) and $MLH3^{D1223N/D1223N}$ and $MLH3^{E1229K/E1229K}$ cells (Fig. S6). These mutants are hereafter written as $PMS2^{EK/EK}$, $MLH3^{DN/DN}$, and $MLH3^{EK/EK}$ cells. The sensitivity profile of $PMS2^{EK/EK}$ cells was the same as that of $PMS2^{-/-}$ cells (Fig. 1*A*). Likewise, $MLH3^{-/-}$, $MLH3^{DN/DN}$, and $MLH3^{EK/EK}$ cells showed the same phenotype (Fig. 1*B*). These observations suggest that PMS2 and MLH3 contribute to HR-mediated DSB repair as the endonuclease.

The repair of γ-ray–induced DSBs during G_2 phase is severely compromised in the PMS2 and MLH3 mutant cells

To monitor DSB repair selectively during the G_2 phase when HR is active, we exposed cells to ionizing radiation and measured the number of chromosomal aberrations in mitotic chromosome spreads at 3 h after ionizing radiation (59). Only cells that were γ-irradiated at the G_2 phase, but not the S phase, can enter the M phase within 3 h (60). This method allows for evaluating the capability of HR to repair DSBs with several times higher sensitivity than the analysis of the γ-irradiation sensitivity of asynchronous cell populations (Fig. 1, *A* and *B*). Indeed, γ-irradiation increased the number of chromosomal breaks by 1.0 per $MUS81^{-/-}$ cell and only 0.2 per *WT* cell (Fig. 2*B*). Remarkably, the total numbers of chromosome aberrations induced by γ-rays were around 10 times higher in the PMS2 and MLH3 mutant cells compared with *WT* cells (Fig. 2*B*). The total number of mitotic chromosome aberrations was significantly higher in $MLH1^{-/-}$ cells, but not in $MSH2^{-/-}$ cells, compared with *WT* cells (Fig. 2*B* and Fig. S4*K*). We conclude that there is no significant contribution of canonical MMR involving MSH2 to DSB repair during the G_2 phase. The total numbers of

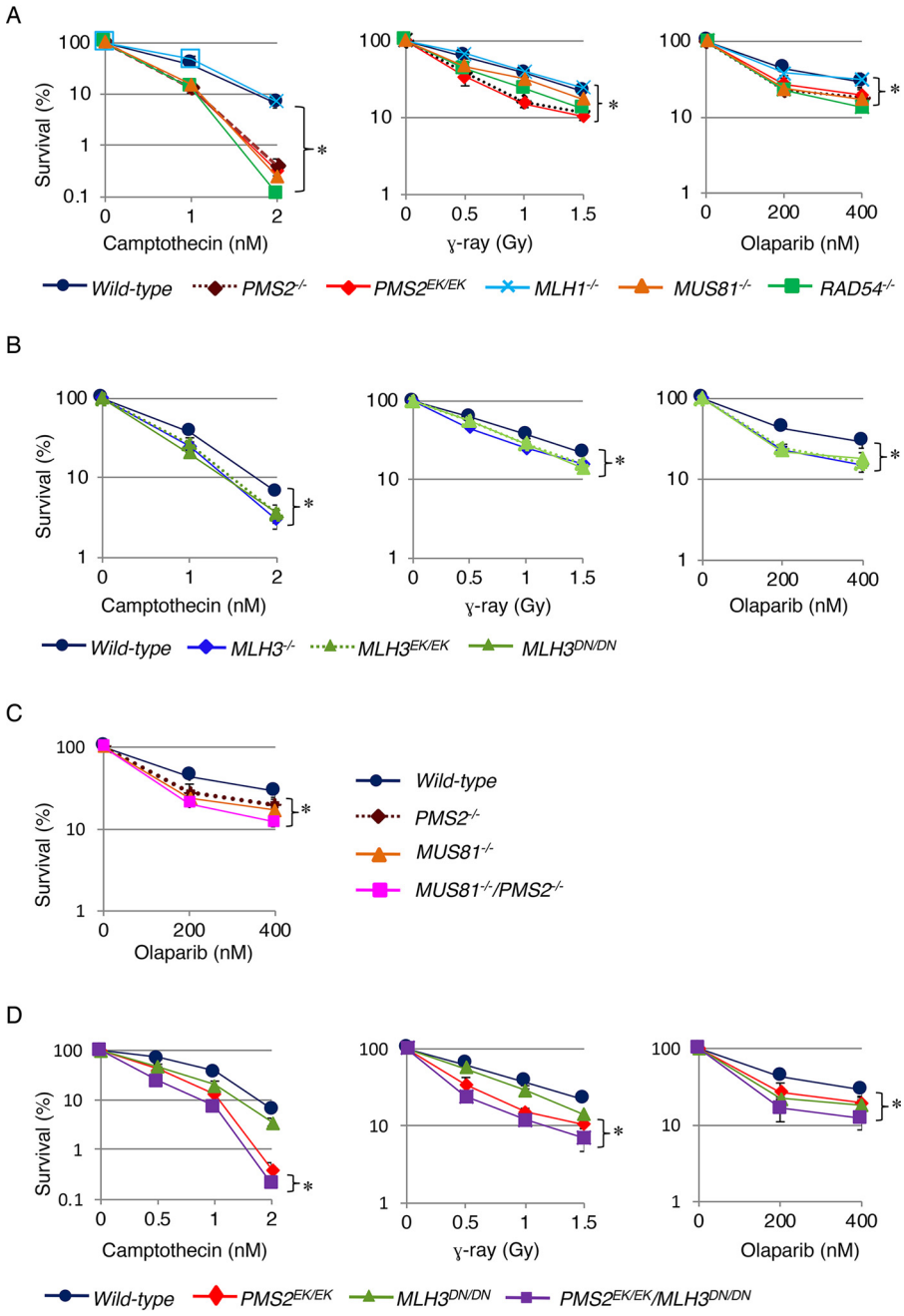

Figure 1. *MLH3* and *PMS2* mutants are sensitive to camptothecin, γ-rays, and olaparib. *A*, clonogenic cell survival assay following exposure of *PMS2* mutants to camptothecin, γ-rays, and olaparib (PARP inhibitor). The *x axis* represents the dose of the indicated DNA-damaging agent on a linear scale; the *y axis* represents the survival fraction on a logarithmic scale. *Error bars*, S.D. for three independent assays. Statistical analyses were performed by Student's *t* test (*, $p < 0.01$). *B*, clonogenic cell survival assay following exposure of *MLH3* mutants to camptothecin, γ-rays, and olaparib (PARP inhibitor). Cellular sensitivity is shown as in *A*. Statistical analyses were performed by Student's *t* test (*, $p < 0.01$). *C*, clonogenic cell survival assay following exposure of $MUS81^{-/-}PMS2^{-/-}$ mutants to olaparib (PARP inhibitor). Cellular sensitivity is shown as in *A*. *D*, $PMS2^{EK/EK}/MLH3^{DN/DN}$ double mutant cells show stronger HR defects than $PMS2^{EK/EK}$ and $MLH3^{DN/DN}$ cells. Shown is a clonogenic cell survival assay following exposure of $PMS2^{EK/EK}$, $MLH3^{DN/DN}$, and $PMS2^{EK/EK}MLH3^{DN/DN}$ mutants to camptothecin, γ-rays, and olaparib (PARP inhibitor). Cellular sensitivity is shown as in *A*. Statistical analyses were performed by Student's *t* test (*, $p < 0.05$).

γ-ray–induced chromosome aberrations increased to very similar extents in the five mutants, $PMS2^{-/-}$, $PMS2^{EK/EK}$, $MLH3^{-/-}$, $MLH3^{DN/DN}$, and $MLH3^{EK/EK}$ cells (Fig. 2*B*). These data suggest that PMS2 and MLH3 significantly contribute to DSB repair as endonuclease.

We counted the number of chromosome aberrations distinguishing chromatid-type breaks (where one of the two sister chromatids is broken), isochromatid-type breaks (where two sister chromatids are broken at the same sites), and radial chromosomes (which comprise the association of two or more chromatids) (Fig. 2*A*). Ionizing irradiation of $RAD54^{-/-}$ cells caused a more significant increase in the number of chromatid-type breaks than that of isochromatid-type breaks (Fig. 2*B*). This observation agrees with the role of Rad54 in promoting strand exchange and JM formation. In contrast, $MUS81^{-/-}$ cells showed marked increases in the numbers of isochromatid-type

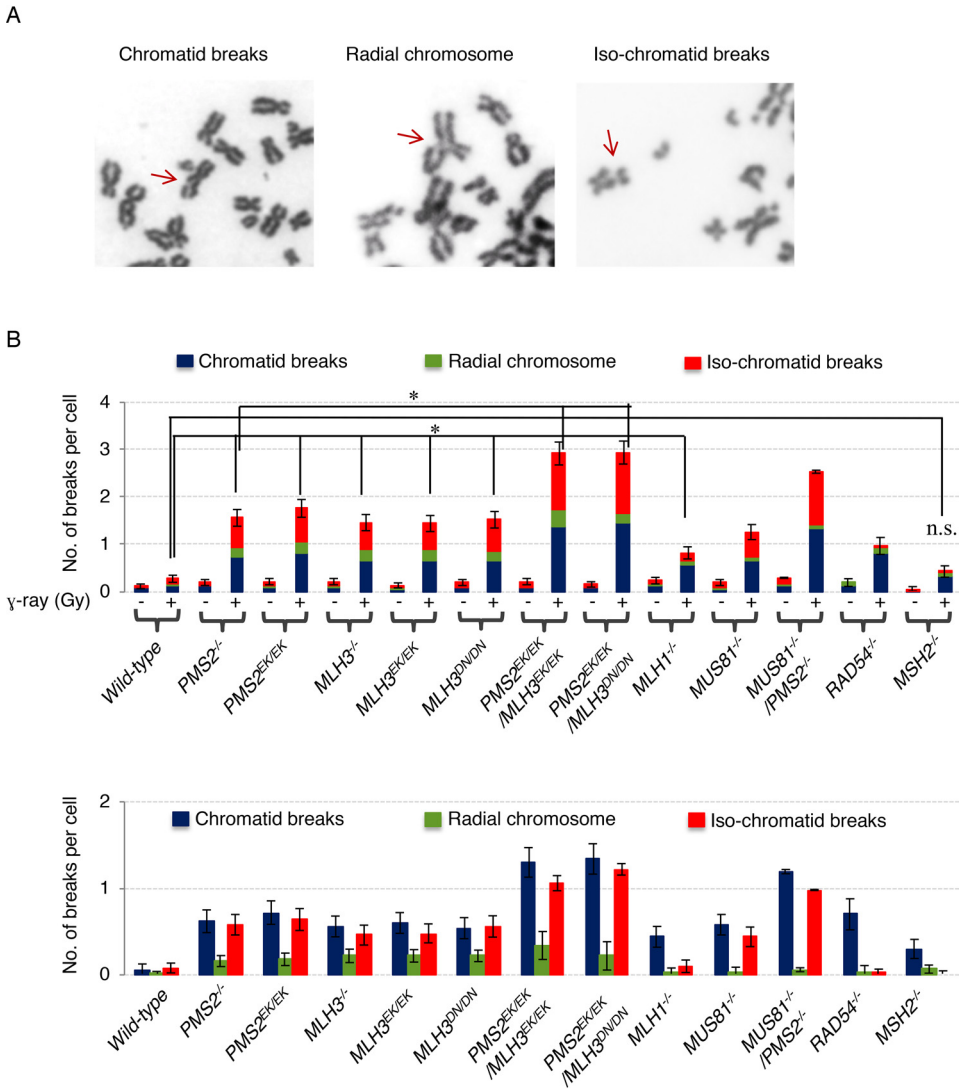

Figure 2. HR-mediated repair of γ-ray–induced DSBs is severely compromised in the PMS2 and MLH3 mutant cells. *A*, representative images of chromatid breaks, isochromatid breaks, and radial chromosome after irradiation of 1-Gy IR. *B*, number of breaks per mitotic cell in the indicated genotypes (*top*). *Error bars*, S.D. The *asterisks* indicate $p < 0.001$, calculated by Student's *t* test. At least 50 mitotic cells were counted for each cell line. The number of breaks before the exposure was subtracted from breaks after the exposure (*bottom*). *Error bars*, propagation of error.

breaks. Isochromatid-type breaks result from abnormal processing of JMs between broken and intact sister chromatids, as the persistent presence of JMs interferes with local chromosome condensation of both sister chromatids, leading to microscopically visible breakage of the two chromosomes at the same sites (39, 61, 62). Radial chromosomes may be caused by the abnormal separation of JMs containing two sisters, leading to inverted chromosome fusions. Like $MUS81^{-/-}$ cells, the PMS2 and MLH3 mutants showed significant increases in the numbers of both isochromatid-type breaks and radial chromosomes (Fig. 2*B*). These data suggest that PMS2 and MLH3 promote HR-dependent DSB repair after formation of JMs as does MUS81.

Surprisingly, the $MLH1^{-/-}$ phenotype is not as severe as expected from the phenotypes of the PMS2 and MLH3 mutants, particularly no significant alteration regarding isochromatid-type breaks. A moderate increase in the number of chromatid-type breaks in $MLH1^{-/-}$ cells suggests that the MLH1-MLH3 and MLH1-PMS2 heterodimers may play a minor role in NHEJ-mediated DSB repair, as suggested previously (19). One possible scenario is that an MLH1-independent alternative mechanism of PMS2 and MLH3 might be present in the process observed in this study. These data suggest that PMS2 and MLH3 promote HR-dependent DSB repair after the formation of JMs, as does MUS81.

$PMS2^{EK/EK}/MLH3^{DN/DN}$ double mutant cells display stronger HR defects than $PMS2^{EK/EK}$ and $MLH3^{DN/DN}$ cells

We chose $MLH3^{DN/DN}$ cells as a representative MLH3 mutant due to the phenotypic similarity among $MLH3^{-/-}$, $MLH3^{DN/DN}$, and $MLH3^{EK/EK}$ cells. Likewise, we chose $PMS2^{EK/EK}$ cells for the subsequent analyses. To investigate the functional relationship between the PMS2 and MLH3 endonucleases, we generated $PMS2^{EK/EK}/MLH3^{DN/DN}$ double mutant cells. The doubling time was 12.5 h for *WT*, 12.7 h for $PMS2^{EK/EK}$, 12.7 h

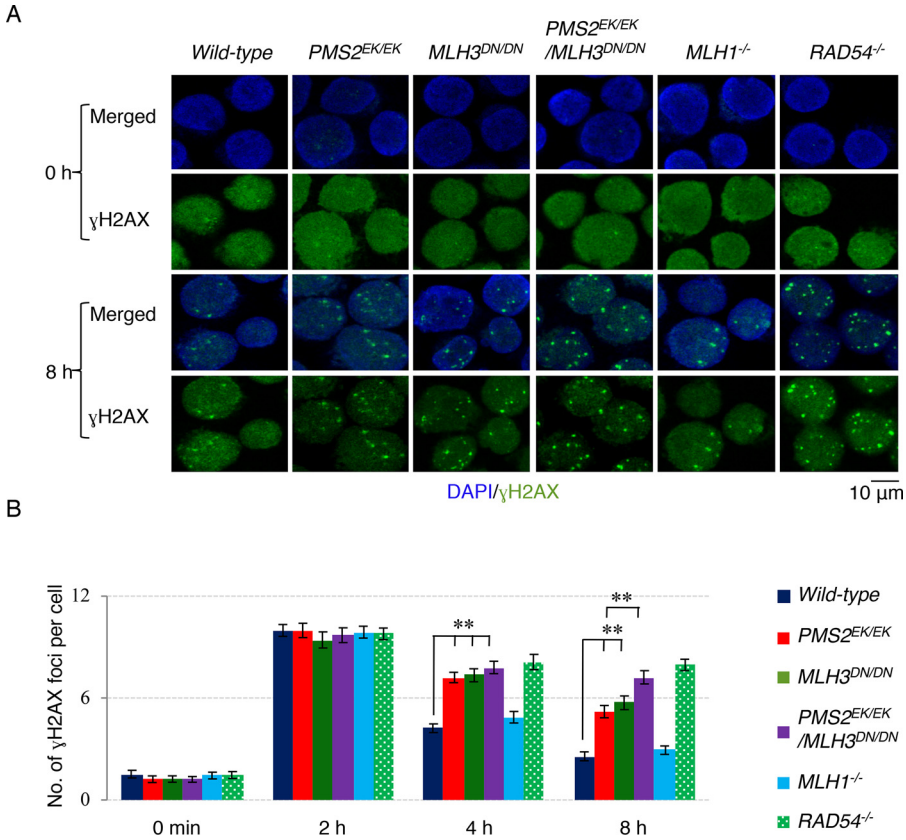

Figure 3. Following ionizing radiation, γH2AX foci appear with normal kinetics but persist for a longer time in the *PMS2* and *MLH3* mutants compared with WT cells. *A*, representative fluorescence microscopic images of γH2AX foci in the indicated cell lines before and 8 h after irradiation of 1-Gy IR. *Green specks*, γH2AX signal; *blue*, nuclei. *DAPI*, 4′,6-diamidino-2-phenylindole. *B*, quantification of number of γH2AX foci/cell at the indicated time points. At least 100 cells were counted per condition in each experiment. Statistical analyses were performed by Student's *t* test (**, $p < 0.001$).

for $MLH3^{DN/DN}$, and 14.3 h for $PMS2^{EK/EK}/MLH3^{DN/DN}$ cells. The plating efficiency of these cells was 50–60% for all genotypes. $PMS2^{EK/EK}/MLH3^{DN/DN}$ cells showed high sensitivity to camptothecin and γ-rays, higher than $MLH3^{DN/DN}$ and slightly higher than $PMS2^{EK/EK}$, suggesting a prominent role of PMS2 in these assays (Fig. 1*D*). $PMS2^{EK/EK}/MLH3^{DN/DN}$ cells also showed a higher sensitivity to olaparib than did $PMS2^{EK/EK}$ and $MLH3^{DN/DN}$ cells (Fig. 1*D*). The number of γ-ray–induced chromosomal breaks was more than 50% higher in $PMS2^{EK/EK}/MLH3^{DN/DN}$ cells than in $PMS2^{EK/EK}$ and in $MLH3^{DN/DN}$ cells (Fig. 2). We therefore conclude that PMS2 and MLH3 contribute to HR as the endonuclease independently of each other.

We monitored DSB repair kinetics by measuring the number of γH2AX foci with time after γ-irradiation (Fig. 3). The numbers of γH2AX foci were very similar among $MLH3^{DN/DN}$, $PMS2^{EK/EK}$, and *WT* cells at 2 h after ionizing irradiation. The numbers of γH2AX foci reduced more slowly in $MLH3^{DN/DN}$ and $PMS2^{EK/EK}$ cells compared with *WT* and $MLH1^{-/-}$ cells (Fig. 3). The delayed DSB repair kinetics observed more than 2 h after ionizing irradiation is consistent with the fact that HR needs a longer time to complete DSB repair than does NHEJ (20). $PMS2^{EK/EK}/MLH3^{DN/DN}$ cells showed a more prominent delay in DSB repair at 8 h compared with $MLH3^{DN/DN}$ and $PMS2^{EK/EK}$ cells (Fig. 3). We conclude that PMS2 and MLH3 promote DSB repair independently of each other in an MLH1-independent manner.

Resolution of γ-ray–induced Rad51 foci is delayed in the PMS2 and MLH3 mutant cells

To evaluate whether PMS2 and MLH3 act in the early and late steps of HR, we analyzed the formation of Rad51 foci over time after γ-irradiation (Fig. 4). The number of Rad51 foci peaked at 2 h after γ-irradiation in *WT* TK6 cells (59, 60). $MLH3^{DN/DN}$, $PMS2^{EK/EK}$, and $PMS2^{EK/EK}/MLH3^{DN/DN}$ cells showed the same extent of Rad51 foci at 2 h as *WT* cells. Thus, PMS2 and MLH3 are dispensable for DSB resection and the polymerization of Rad51 on resected DSBs. Remarkably, $MLH3^{DN/DN}$, $PMS2^{EK/EK}$, and $PMS2^{EK/EK}/MLH3^{DN/DN}$ cells showed a significant delay in the resolution of Rad51 foci compared with *WT* and $MLH1^{-/-}$ cells (Fig. 4). Both $MLH3^{DN/DN}$ and $PMS2^{EK/EK}$ single mutants showed a similar delay in the resolution of Rad51 foci compared with $MUS81^{-/-}$ cells, but this effect was more prominent in the $PMS2^{EK/EK}/MLH3^{DN/DN}$ double mutant cells (Fig. 4*B*). All mutants were less sensitive than $RAD54^{-/-}$ cells. We therefore conclude that the PMS2 and MLH3 endonucleases promote HR-dependent DSB repair after the polymerization of Rad51 at DSBs.

$MLH3^{DN/DN}$ and $PMS2^{EK/EK}$ cells are deficient in heteroallelic HR

To assess the involvement of PMS2 and MLH3 in the resolution of HJs, we measured the frequency of heteroallelic recombination between the allelic thymidine kinase (*TK*) genes

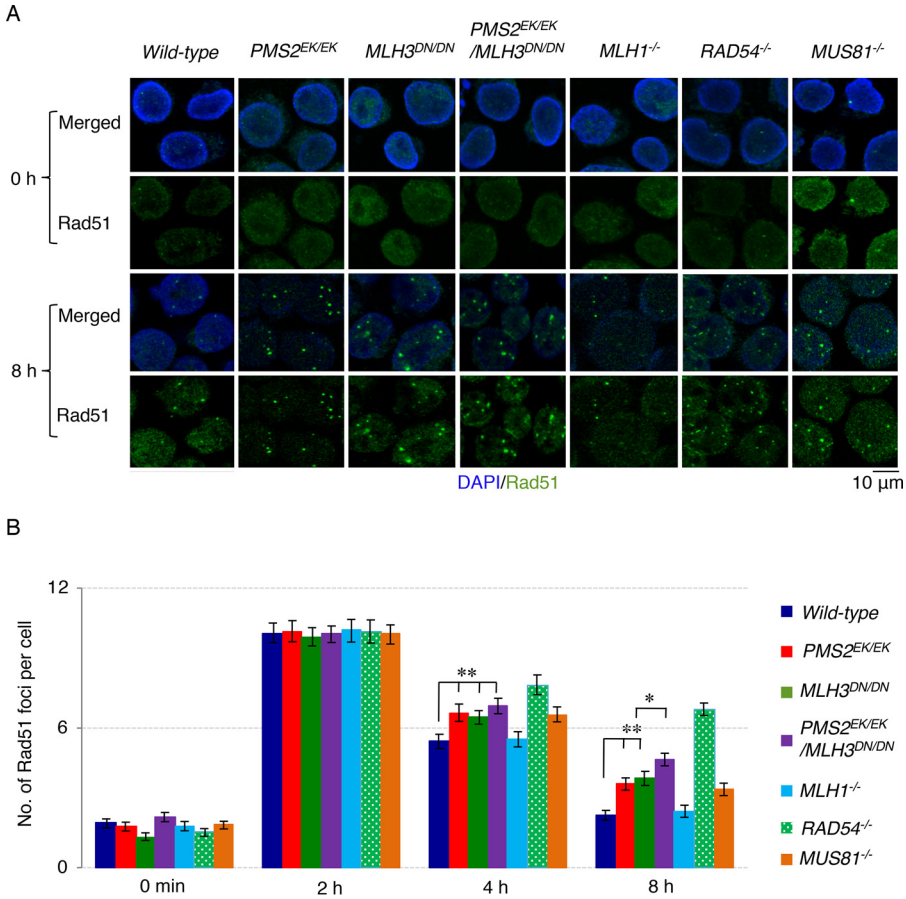

Figure 4. Following ionizing radiation, Rad51 foci appear with normal kinetics but persist for a longer time in the *PMS2* and *MLH3* mutants compared with WT cells. *A*, representative fluorescence microscopic images of Rad51 foci in the indicated cell lines before and 8 h after irradiation of 1-Gy IR. *Green specks*, Rad51 signal; *blue*, nuclei. *DAPI*, 4′,6-diamidino-2-phenylindole. *B*, quantification of the number of Rad51 foci/cell at the indicated time points. At least 100 cells were counted per condition in each experiment. Statistical analyses were performed by Student's *t* test (*, $p < 0.01$; **, $p < 0.001$).

carrying compound heterozygous mutations (47, 50, 60, 63) (Fig. 5*A*). One of the two allelic *TK* genes carries an I-SceI site, and a mutation in the exon 5 localizes 108 nucleotides downstream of the I-SceI site. When I-SceI–induced DSBs are repaired by either the gene conversion (HR) that associates with crossover or long-tract gene conversion, it can restore an intact *TK* gene. These restoration events are detectable by counting the frequency of drug-resistant colonies (50). The HR frequency was 60% lower in $MUS81^{-/-}$ cells compared with *WT* cells (Fig. 5*B*), suggesting that a majority of the heteroallelic recombination events involve the formation of HJs. The PMS2 and MLH3 mutants, including $MLH3^{DN/DN}$ and $PMS2^{EK/EK}$ cells, showed 60–70% decreases, and $PMS2^{EK/EK}/MLH3^{DN/DN}$ and $MUS81^{-/-}/PMS2^{-/-}$ cells showed further declines in the frequency of crossover events when compared with *WT* cells (Fig. 5*B*). These observations suggest that the endonuclease activity of PMS2 and MLH3 may be involved in the resolution of HJs. This function of PMS2 and MLH3 is also independent of MLH1 and MSH2.

We further assessed the involvement of PMS2 and MLH3 in the resolution of HJs by measuring SCE events, crossover-type HR (62, 64, 65). To induce SCE, we treated cells with cisplatin, an interstrand cross-linking agent. The number of cisplatin-induced SCE events was measured by subtracting the number of SCEs before cisplatin treatment from the number of SCEs post-treatment (Fig. 5, *C* and *D*). The treatment increased the SCE frequency by 11 events per 100 mitotic *WT* cells (Fig. 5*D*). The number of induced SCEs was 50% smaller in $MUS81^{-/-}$ cells when compared with *WT* cells. $MLH3^{DN/DN}$ and $PMS2^{EK/EK}$ cells also showed 50% decreases, and $PMS2^{EK/EK}/MLH3^{DN/DN}$ cells showed an 80% decrease in the SCE compared with *WT* cells (Fig. 5, *C* and *D*). In summary, PMS2 and MLH3 contribute to crossover formation most likely by promoting the resolution of HJs, as does MUS81, but MLH1 is not involved in this process.

The loss of MLH1 does not impair HR-dependent DSB repair

MLH1 physically interacts with PMS2 and MLH3 as heterodimers and thereby stabilizes the two endonucleases (66). Here, to evaluate the role of MLH1 in the mitotic HR, we have employed five phenotypic assays: (i) sensitivity to camptothecin, γ-irradiation, and olaparib (Fig. 1*A* and Fig. S4*J*), (ii) γ-ray–induced chromosome aberrations (Fig. 2*B* and Fig. S4*K*), (iii) measuring the number of γH2AX and Rad51 foci over time after γ-irradiation (Figs. 3 and 4), (iv) measuring the frequency of the heteroallelic recombination (Fig. 5, *A* and *B*), and (v) SCE induced by cisplatin (Fig. 5, *C* and *D*). Unexpectedly, as mentioned above, all of these phenotypic assays consistently showed that $MLH1^{-/-}$ cells were proficient in HR-mediated

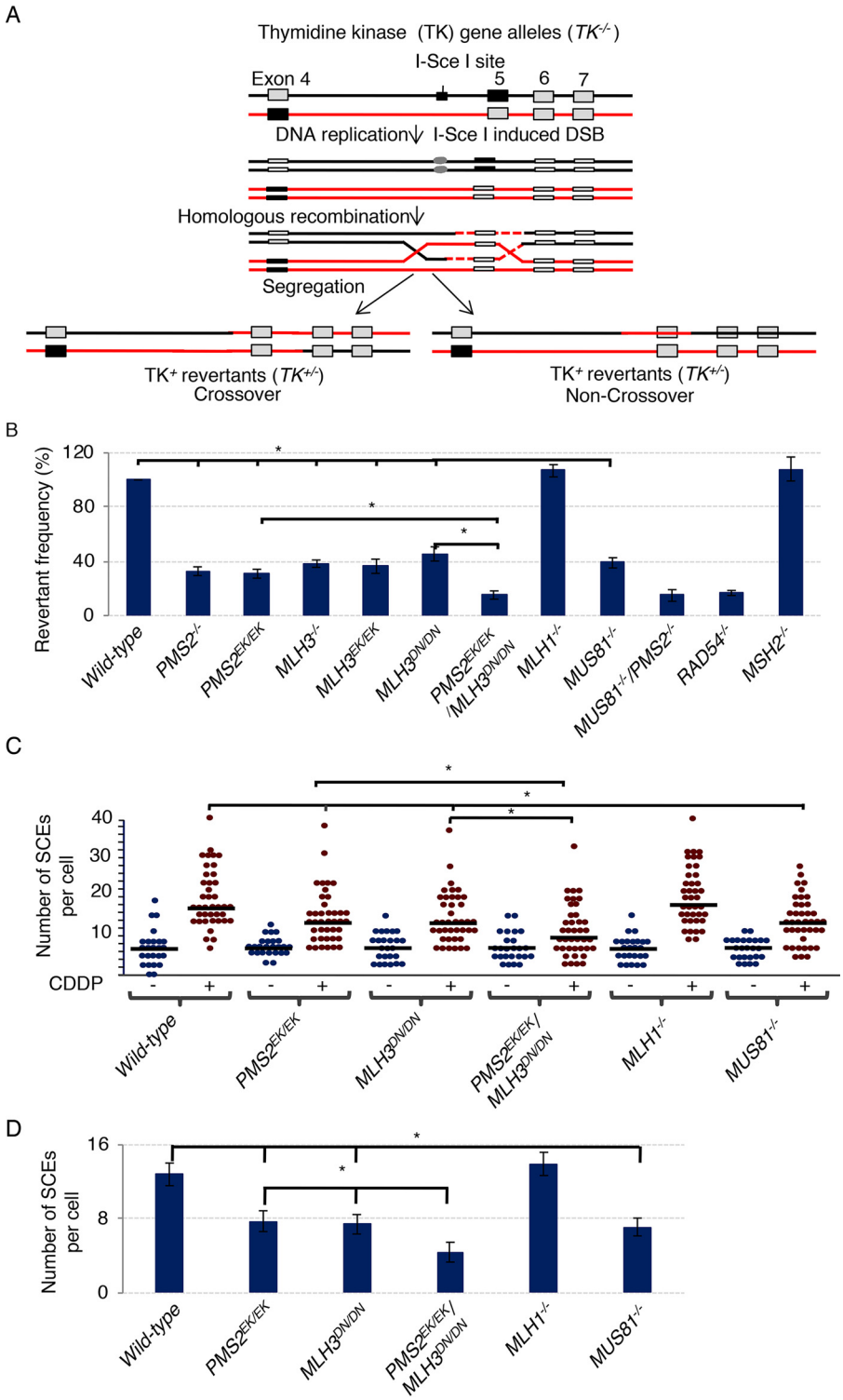

Figure 5. *MLH3*$^{DN/DN}$ and *PMS2*$^{EK/EK}$ cells are deficient in HR associated with crossover. *A*, schematic diagram showing DSB repair events that repair I-SceI–induced DSBs in the endogenous *TK* locus. *TK*$^{-/-}$ cells carry an I-SceI site in intronic sequences of the *TK* allelic gene. The sites of mutations in the *TK* allelic genes are marked as *closed rectangles* at exon 4 and exon 5. When a DSB at the I-SceI site is repaired by HR, TK-proficient revertants (TK$^{+/-}$) are generated by crossover resolution from TSCER2 cells under CHAT selection. *B*, histogram representing the frequency of DSB repair events (*y axis*) in the indicated genotypes (*x axis*). *Error bars*, S.D. of more than three independent experiments. Statistical analyses were performed by Student's *t* test ($p < 0.01$). *C*, nuclease-dead *PMS2* and *MLH3* mutants displayed a reduced number of SCE events induced by cisplatin (*CDDP*). The distribution of SCE events per 100 chromosomes is shown for the indicated cell types. Mean values for SCE before and after exposure to the DNA-damaging agents are indicated. Statistical analyses were performed by Student's *t* test ($p < 0.01$). *D*, the number of SCEs before the exposure was subtracted from SCEs after the exposure. *Error bars*, S.E. Statistical analyses were performed by Student's *t* test ($p < 0.01$).

DSB repair. We therefore conclude that MLH1 is dispensable for the functioning of human MLH3 and PMS2 in mitotic HR. It represents to our knowledge the first example where MLH1 is not required for the functioning of MLH3 and PMS2. Indeed, MLH1 has been shown to be required for the functioning of MLH3 and PMS2 in MMR and in meiotic HR in mice (24, 25).

We speculated that the MLH1-independent function of PMS2 and MLH3 in mitotic HR can be achieved through (i) homodimer formation, (ii) formation of a heterodimer with an unknown partner protein, which would stabilize the PMS2 and MLH3 proteins, and (iii) formation of an MLH3-PMS2 heterodimer. We could not examine these possibilities due to the lack of specific antibodies and no appropriate method of inserting functional tag sequences into PMS2 and MLH3. We therefore investigated PMS2 and MLH3 homodimer and heterodimer formation through 3D structure modeling using a standard homology modeling pipeline based on the HHpred and RosettaCM methods (67–69). Structural analysis of the resulting models supports the potential homodimer and heterodimer formation (Fig. S8, *A*–*C*).

Significant rescue of the defective HR of the MLH3 and PMS2 mutants by ectopic expression of GEN1

We reason that if the PMS2 and MLH3 endonuclease activities promote HR by processing HJs, the mutant phenotype of $MLH3^{DN/DN}$ and $PMS2^{EK/EK}$ cells could be suppressed by ectopic expression of one of the resolvases described for HJs. We chose GEN1 as the HJ resolvase (70) and used the *GEN1* transgene carrying mutations in its nuclear export signal (NES) and fused with the nuclear localization signal (NLS) (71) (Fig. 6*A*). We added the FLAG tag to this *GEN1* transgene and inserted it into the pMSCV retroviral expression vector, which allows for the bicistronic expression of the *GFP* and *GEN1* transgenes (72) (Fig. S7). We produced recombinant retrovirus and infected them into TK6 clones. To confirm the expression of the transgene, we performed Western blotting analyses using an anti-FLAG antibody (Fig. S7*D*). We measured the ionizing radiation sensitivity and calculated LD_{50}, the dose of γ-rays that reduced the survival of cells to 50% relative to nonirradiated cells (Fig. 6*B*). The expression of the *GEN1* transgene reversed the ionizing radiation sensitivity of $MUS81^{-/-}$ cells, but not *WT* or $RAD54^{-/-}$ cells. Thus, the *GEN1* transgene is able to selectively normalize the defective processing of JMs during HR-mediated DSB repair.

The *GEN1* transgene restored the tolerance of $MLH3^{DN/DN}$, $PMS2^{EK/EK}$, and $PMS2^{EK/EK}/MLH3^{DN/DN}$ cells to γ-rays at least partially (Fig. 6*B*). The rescue effect of *GEN1* transgene was more efficient in $PMS2^{EK/EK}/MLH3^{DN/DN}$ double mutant cells compared with $MLH3^{DN/DN}$ and $PMS2^{EK/EK}$ cells. In agreement with this finding, the *GEN1* transgene significantly reduced the total number of chromosomal aberrations in these mutants as well as $MUS81^{-/-}$ cells (Fig. 6*C*). Importantly, the *GEN1* transgene expression reduced the number of isochromatid-type breaks to a considerably greater extent than that of chromatid breaks (Fig. 6*C*). The *GEN1* transgene increased the frequency of heteroallelic HR in $MUS81^{-/-}$ cells by 60% but had no effect on that in *WT* or $RAD54^{-/-}$ cells (Fig. 6*D*), suggesting that a substantial fraction of heteroallelic HR involves HJ formation as HR intermediates. The *GEN1* transgene restored heteroallelic HR in $MLH3^{DN/DN}$, $PMS2^{EK/EK}$, $PMS2^{EK/EK}/MLH3^{DN/DN}$, and $MUS81^{-/-}$ cells but not *WT* or $RAD54^{-/-}$ cells (Fig. 6*D*). In summary, the PMS2 and MLH3 endonuclease activities facilitate the separation of HJs.

Discussion

We demonstrate that human PMS2 and MLH3 promote DSB repair by HR in human somatic cells. Previous studies failed to uncover their role in the repair of X-ray-induced DSBs, presumably because murine primary cells deficient in PMS2 are slightly resistant to ionizing radiation due to defective MMR of damaged nucleotides (73). Strikingly, the defective HR phenotype of the PMS2 and MLH3 mutants derived from the TK6 cell line was as prominent as that of TK6 cells deficient in MUS81, an important endonuclease involved in the resolution of HJs (36, 37) (Figs. 2*B* and 5 (*B*, *C*, and *D*)). Furthermore, $PMS2^{EK/EK}/MLH3^{DN/DN}$ cells displayed a significantly stronger phenotype than did $MUS81^{-/-}$ cells, including 15 times more mitotic chromosome breaks induced by γ-irradiation at the G_2 phase (Fig. 2*B*) and an ∼80% decrease in the number of cisplatin-induced sister chromatic exchanges (Fig. 5, *C* and *D*) compared with *WT* cells. The contribution of PMS2 and MLH3 to HR is totally independent of their functioning in MMR because MSH2 and MLH1 are required for MMR but dispensable for HR (Fig. 2). In summary, human PMS2 and MLH3 significantly contribute to the genome stability of somatic cells through at least two distinct mechanisms: MMR and DSB repair by HR.

The present study shows compelling genetic evidence for the requirement of the PMS2 and MLH3 endonuclease activity for the efficient resolution of HJs. $MLH3^{DN/DN}$ and $MLH3^{-/-}$ cells showed the same phenotype in the defective HR (Fig. 2). Likewise, the phenotype of $PMS2^{EK/EK}$ cells was very similar to that of $PMS2^{-/-}$ cells (Fig. 2). These data indicate that PMS2 and MLH3 promote HR as the endonuclease. In the $MLH3^{DN/DN}$ and $PMS2^{EK/EK}$ mutants, the initial kinetics of γ-ray–induced Rad51 focus formation was normal, whereas its resolution was significantly delayed (Fig. 4). We therefore conclude that the PMS2 and MLH3 endonuclease activities promote a late step of HR, most likely after the formation of JMs. The $MUS81^{-/-}$, $MLH3^{DN/DN}$, and $PMS2^{EK/EK}$ mutants all showed a ∼40% decrease in the frequency of cisplatin-induced SCEs (Fig. 5*D*). Furthermore, ectopic expression of GEN1, a typical HJ resolvase, reversed the defective heteroallelic HR of $MUS81^{-/-}$, $MLH3^{DN/DN}$, and $PMS2^{EK/EK}$ cells by 30–50% (Fig. 6). In conclusion, the endonuclease activity of PMS2 and MLH3 process HJs, generating both crossover and noncrossover products.

The PMS2-MLH1 and MLH3-MLH1 heterodimers are involved in both MMR and meiotic HR in *S. cerevisiae* and mice (21, 24, 25, 66). Unexpectedly, we observed that only PMS2 and MLH3, and not MLH1, are involved in HR in human somatic cells. The PMS2 and MLH3 proteins may form homodimers and heterodimers when they are involved in HR in the same manner as the MutL homologs form heterodimer mediated by their C-terminal region (14). Indeed, homodimers of yeast Mlh1 have been reported, and an increase of their formation can inhibit MMR (74). In addition, in support of a possible heterodimer formation, a recent study in budding yeast found co-immunoprecipitation of Mlh3 with Pms1 (75). The crystal structure of the C-terminal region of human MLH1 (Protein Data Bank code 3RBN) showed that human MLH1 could form homodimers with the same

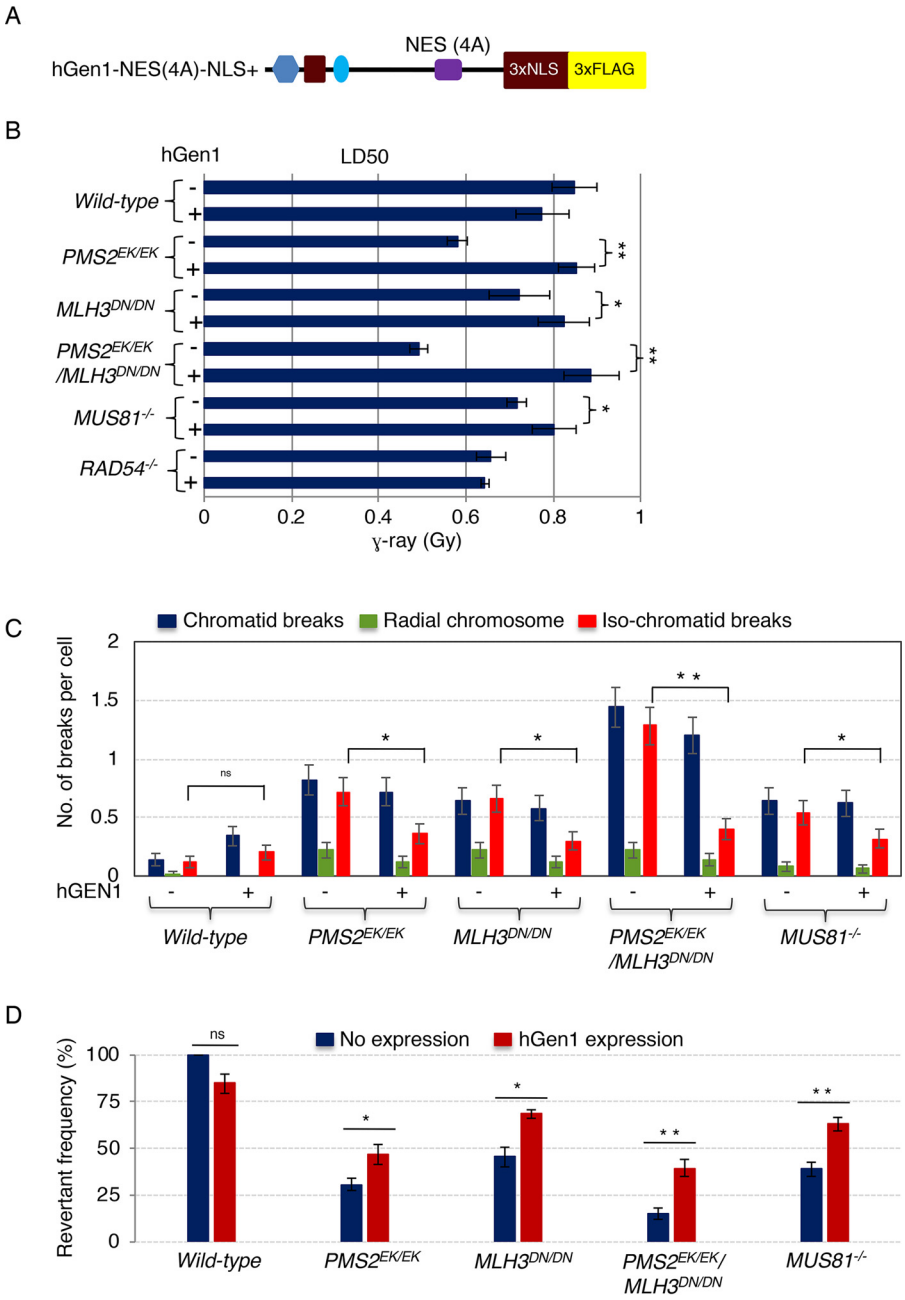

Figure 6. Significant rescue of the defective HR of the *MLH3* and *PMS2* mutants by ectopic expression of GEN1. *A*, schematic representation of hGEN1 with a mutated NES and 3xNLS sequences. *B*, clonogenic cell survival of the indicated DNA-damaging agents was analyzed as described in the legend to Fig. 1*A*. Lethal dose 50% (LD_{50}) is the concentration of DNA-damaging agents that reduces cellular survival to 50% relative to cells not treated with DNA-damaging agents. *Error bars*, S.D. of at least three independent experiments. Statistical analyses were performed by Student's *t* test (*, $p < 0.05$; **, $p < 0.01$). *C*, number of IR-induced chromosomal aberrations per mitotic cell in the indicated genotypes. *Error bars*, S.D. At least 50 mitotic cells were counted for each cell line. Statistical analyses were performed by Student's *t* test (*, $p < 0.05$; **, $p < 0.01$; *ns*, not significant). *D*, frequency of heteroallelic HR associated with crossover was measured and calculated as described in the legend to Fig. 5*B*. Statistical analyses were performed by Student's *t* test (*, $p < 0.05$; **, $p < 0.01$; *ns*, not significant).

residues involved in the heterodimer formation (14). The HHpred and RosettaCM analysis also suggested that both the homodimer and heterodimer formation are possible (Fig. S8). Future studies will demonstrate the homodimer and heterodimer formation as well as the interaction with an unidentified partner protein.

MLH3 and PMS2 have strong tumor suppressor activities, and it is believed that these activities are attributable exclusively to their function of MMR (76). The current study suggests that these endonucleases may contribute to tumor suppression also by promoting the resolution of HJs. The MUS81-EME1, SLX1-SLX4, and GEN1 endonucleases all play a critical role in genome maintenance, particularly when Bloom helicase is attenuated (62, 77, 78). Nonetheless, it remains unclear how much these endonucleases contribute to tumor suppression in humans. A defect in the resolution of HJs can pose a more serious threat to genome stability compared with the initial step of HR because the former deficiency not only leaves DSBs unrepaired but also can cleave intact sister chromatids (79). The following two mouse experiments suggest the critical role played

Table 1
Panel of cell lines used in this study

Genotype	Parental cell line	Marker genes	Sources
PMS2$^{-/-}$	TK6	*hygro*^{R}, *puro*^{R}	TALEN (this work)
PMS2$^{EK/EK}$	TK6		CRISPR (this work)
MLH3$^{-/-}$	TK6	*hygro*^{R}, *neo*^{R}	CRISPR (this work)
MLH3$^{DN/DN}$	TK6		CRISPR (this work)
MLH3$^{EK/EK}$	TK6		CRISPR (this work)
PMS2$^{EK/EK}$ *MLH3*$^{DN/DN}$	TK6		CRISPR (this work)
PMS2$^{EK/EK}$ *MLH3*$^{EK/EK}$	TK6		CRISPR (this work)
MUS81$^{-/-}$	TK6	*bsr*^{R}, *puro*^{R}	TALEN (this work)
RAD54$^{-/-}$	TK6	*neo*^{R}, *puro*^{R}	TALEN (47)
MLH1$^{-/-}$	TK6	*hygro*^{R}, *puro*^{R}	CRISPR (this work)
MSH2$^{-/-}$	TK6	*neo*^{R}, *puro*^{R}	CRISPR (this work)

by HJ resolvases in tumor suppression. SLX4 serves as a docking site for MUS81-EME1, SLX1-SLX4, and XPF-ERCC1 endonucleases and MSH2-MSH3 mismatch repair factor (79). SLX4 plays a dominant role in preventing carcinogenesis, as evidenced by the data indicating that the loss of SLX4 decreases the median survival time of mice to ~90 days due to enhanced tumorigenesis (80). The *MUS81* null mutation reduces the life expectancy of p53 null mice by about 30% due to an increase in carcinogenesis (81). The critical role of MLH3 and PMS2 in the resolution of HJs emphasizes their strong tumor suppressor activities in addition to their function in MMR (21, 22, 82).

In this study, we characterized a major role of MLH3 and PMS2 in the DSB repair that is independent of MSH2 and MLH1. These results highlight an additional layer of the multifunctional role played by the MMR proteins (66). Studies on the molecular mechanisms of the process identified here will allow determination of whether this process is mediated by the homodimeric form of PMS2 and MLH3, a complex with not yet characterized partners, or a new pathway of DSB repair.

Experimental procedures

Cell clones

All of the clones used in this study are summarized in Table 1.

Cell culture

Cell culture conditions for human TK6 cells were as described previously (83). Briefly, TK6 cells were grown in RPMI 1640 medium (Nacalai Tesque Inc., Kyoto, Japan) supplemented with 10% heat-inactivated horse serum (Gibco, Life Technologies New Zealand, Ltd., Auckland, New Zealand), 200 μg/ml sodium pyruvate, and 100 units/ml penicillin plus 100 μg/ml streptomycin at 37 °C in 5% CO_2 atmosphere.

Generation of human *PMS2*$^{-/-}$ TK6 B cells

To generate a pair of TALEN expression plasmids against the *PMS2* gene, we used a Golden Gate TALEN kit and a TAL effector kit (Addgene) (84, 85). The TALEN target sites are shown in Fig. S1*A*. The gene-targeting constructs were generated from the genomic DNA of TK6 cells by amplifying with primers HindIII-flanked F1 and HindIII-flanked R1 for the 5′-arm and XbaI-flanked F2 and XbaI-flanked R2 for the 3′-arm. The 5′-arm and 3′-arm PCR products were cloned into the corresponding sites of the DT-ApA/puro or DT-ApA/hygro vectors. 10 μg of TALEN expression plasmids and 10 μg of linearized gene-targeting vectors were transfected into 10×10^6 TK6 cells using the Bio-Rad Gene Pulser II Transfection System at 250 V and 950 microfarads. After electroporation, cells were released into 20 ml of drug-free medium containing 10% horse serum. 48 h later, cells were seeded into 96-well plates with both hygromycin and puromycin antibiotics for 2 weeks. The gene disruption was confirmed by genomic PCR using primers P1, P2, P3, of P4 (Fig. S1*B*) and RT-quantitative PCR using primers P5 and P6 (Fig. S1*C*). All primers used in this study are shown in Table S1.

Generation of nuclease-dead human *PMS2*$^{E705K/E705K}$ TK6 B cells

To generate nuclease-dead human *PMS2*$^{E705K/E705K}$ TK6 B cells, we designed a guide RNA targeting intron sequence upstream of the 12th exon using the Zhang CRISPR tool (86) and gene-targeting constructs. The CRISPR target site is depicted in Fig. S1*C*. The gene-targeting constructs were generated using SLiCE (seamless ligation cloning extract). The genomic DNA was amplified with primers F3 and R3 from the *PMS2* gene locus, and the PCR product was used as template DNA for amplifying the 5′-arm. The 5′-arm was amplified using primers F4 and R4, where each primer shared 20-bp end homology with the insertion site of the vector. The sequence intended as the 3′-arm of the *PMS2*-targeting construct was amplified by PCR as two fragments using overlapping primers (F5 and R5) and included a point mutation to change codon 705 from glutamic acid to lysine. The two fragments were then combined by chimeric PCR to yield the 3′ targeting arm including the codon 705 mutation. The 3′-arm was amplified using primers F6 and R6, where each primer shared 20-bp end homology with the insertion site of the vector. Both vectors, DT-ApA/neo and DT-ApA/hygro, were linearized with NotI and XbaI. All of the fragments of the vectors and inserts were purified using a QIAquick gel extraction kit (Qiagen, Venlo, Netherlands). The gene-targeting constructs were generated in a single reaction mixture containing DT-ApA/neo or DT-ApA/hygro vectors, 5′- and 3′-arms, and 2× SLiCE buffer (Invitrogen) and incubated for 30 min at room temperature. 6 μg of CRISPR and 2 μg of each gene-targeting vector were transfected into 4×10^6 TK6 cells using the Neon Transfection System (Life Technologies, Inc.). After electroporation, cells were released into 20 ml of drug-free medium containing 10% horse serum. 48 h later, cells were seeded into 96-well plates for selection with both neomycin and hygromycin antibiotics for 2 weeks. The gene disruption was confirmed by RT-PCR using primers F7 and R7 followed by direct sequencing (Fig. S1, *D* and *E*). The drug resistance markers are flanked by *lox*P sites and were thus excised from *PMS2*$^{E705K/E705K}$ cells by transient expression of Cre recombinase, leading to the generation of *PMS2*$^{E705K/E705K}$ cells.

Generation of human *MLH3*$^{-/-}$ TK6 B cells

To disrupt the *MLH3* gene, we designed a guide RNA targeting the sixth exon using the Zhang CRISPR tool (86) and gene-

targeting constructs. The CRISPR target site is depicted in Fig. S2*A*. The gene-targeting constructs were generated using SLiCE. The genomic DNA was amplified with primers F8 and R8 from the *MLH3* gene locus, and the PCR product was used as template DNA for amplifying the 5′- and 3′-arms. The 5′-arm was amplified using primers F9 and R9, and the 3′-arm was amplified using primers F10 and R10, where each primer shared 20-bp end homology with the insertion site of the vector. Both vectors, DT-ApA/neo and DT-ApA/hygro, were linearized with AflII and ApaI. All of the fragments of the vectors and inserts were purified using a QIAquick gel extraction kit (Qiagen). The gene-targeting constructs were generated in a single reaction mixture containing DT-ApA/neo or DT-ApA/hygro vectors, 5′- and 3′-arms, and 2× SLiCE buffer (Invitrogen) and incubated for 30 min at room temperature. 6 μg of CRISPR and 2 μg of each gene-targeting vector were transfected into 4×10^6 TK6 cells using the Neon Transfection System (Life Technologies). After electroporation, cells were released into 20 ml of drug-free medium containing 10% horse serum. 48 h later, cells were seeded into 96-well plates for selection with both neomycin and hygromycin antibiotics for 2 weeks. The gene disruption was confirmed by RT-PCR using primers F11 and R11 (Fig. S2*B*) and by Southern blotting analysis with a 0.6-kb probe amplified by PCR from genomic DNA using F12 and R12 (Fig. S2*C*). The genomic DNA of the candidate clones was digested with EcoRI for Southern blotting analysis.

Generation of human MSH2$^{-/-}$ TK6 B cells

To disrupt the *MSH2* gene, we designed a guide RNA targeting the fourth exon using the Zhang CRISPR tool (86) and gene-targeting constructs. The CRISPR target site is depicted in Fig. S3*A*. The gene-targeting constructs were generated using SLiCE. The genomic DNA was amplified with primers F22 and R22 from the *MSH2* gene locus, and the PCR product was used as template DNA for amplifying the 5′- and 3′-arms. The 5′-arm was amplified using primers F23 and R23, and the 3′-arm was amplified using primers F24 and R24, where each primer shared 20-bp end homology with the insertion site of the vector. Both vectors, DT-ApA/neo and DT-ApA/puro, were linearized with AflII and ApaI. All of the fragments of the vectors and inserts were purified using a QIAquick gel extraction kit (Qiagen). The gene-targeting constructs were generated in a single reaction mixture containing DT-ApA/neo or DT-ApA/puro vectors, 5′- and 3′-arms, and 2× SLiCE buffer (Invitrogen) and incubated for 30 min at room temperature. 6 μg of CRISPR and 2 μg of each gene-targeting vector were transfected into 4×10^6 TK6 cells using the Neon Transfection System (Life Technologies). After electroporation, cells were released into 20 ml of drug-free medium containing 10% horse serum. 48 h later, cells were seeded into 96-well plates for selection with both neomycin and puromycin antibiotics for 2 weeks. The gene disruption was confirmed by genomic PCR using primers F25, F26, and R25 (Fig. S3).

Generation of human MLH1$^{-/-}$ TK6 B cells

To disrupt the *MLH1* gene, we designed a guide RNA targeting the 8th exon using the Zhang CRISPR tool (86) and gene-targeting constructs. The CRISPR target site is depicted in Fig. S4*A*. The gene-targeting constructs were generated using SLiCE. The genomic DNA was amplified with primers F27 and R27 from the *MLH1* gene locus, and the PCR product was used as template DNA for amplifying the 5′- and 3′-arms. The 5′-arm was amplified using primers F28 and R28, and the 3′-arm was amplified using primers F29 and R29, where each primer shared 20-bp end homology with the insertion site of the vector. Both vectors, DT-ApA/neo and DT-ApA/puro, were linearized with AflII and ApaI. All of the fragments of the vectors and inserts were purified using a QIAquick gel extraction kit (Qiagen). The gene-targeting constructs were generated in a single reaction mixture containing DT-ApA/neo or DT-ApA/puroro vectors, 5′- and 3′-arms, and 2× SLiCE buffer (Invitrogen) and incubated for 30 min at room temperature. 6 μg of CRISPR and 2 μg of each gene-targeting vector were transfected into 4×10^6 TK6 cells using the Neon Transfection System (Life Technologies). After electroporation, cells were released into 20 ml of drug-free medium containing 10% horse serum. 48 h later, cells were seeded into 96-well plates for selection with both neomycin and puromycin antibiotics for 2 weeks. The gene disruption was confirmed by Southern blotting analysis (genomic DNA was digested with SphI) with a 0.52-kb probe amplified by PCR from genomic DNA using F30 and R30 (Fig. S4, *B* and *C*). The candidate clones were further confirmed by RT-PCR using primers F31 and R31 (Fig. S4*D*) and Western blotting analysis (Fig. S4*E*).

Generation of human MUS81$^{-/-}$ TK6 B cells

To generate a pair of TALEN expression plasmids against the *MUS81* gene, we used a Golden Gate TALEN kit and a TAL effector kit (Addgene) (84, 85). The TALEN target sites are shown in Fig. S5*A*. The gene-targeting constructs were generated from the genomic DNA of TK6 cells by amplifying with primers SacI-flanked F19 and BamHI-flanked R19 for the 5′-arm and BamHI-flanked F20 and R20 for the 3′-arm. The 3′-arm PCR products were cloned into pCR-Blunt II-TOPO vector. The 5′-arm PCR products were cloned into the SacI site of the pCR-Blunt II-TOPO vector containing the 3′-arm. The BamHI fragment containing either the bsr^R or $puro^R$ gene was cloned into the BamHI site between the 3′-arm and the 5′-arm in the pCR-Blunt II-TOPO vector. 10 μg of TALEN expression plasmids and 10 μg of linearized gene-targeting vectors were transfected into 10×10^6 TK6 cells using the Bio-Rad Gene Pulser II Transfection System at 250 V and 950 microfarads. After electroporation, cells were released into 20 ml of drug-free medium containing 10% horse serum. 48 h later, cells were seeded into 96-well plates with both blasticidin and puromycin antibiotics for 2 weeks. The genomic DNAs of the isolated clones resistant to both hygromycin and puromycin were digested with DraI for Southern blotting analysis. A 0.6-kb probe was generated by PCR of genomic DNA using primers F21 and R21 (Fig. S5*B*).

Generation of nuclease-dead human $MLH3^{D1223N/D1223N}$ and $MLH3^{E1229K/E1229K}$ TK6 B cells

To generate nuclease-dead human $MLH3^{EK/EK}$ and $MLH3^{DN/DN}$ TK6 B cells, we designed a guide RNA targeting intron sequence upstream of seventh exon using the Zhang CRISPR tool (86) and gene-targeting constructs. The CRISPR target site is depicted in Fig. S6. The gene-targeting constructs were generated using SLiCE. The genomic DNA was amplified with primers F13 and R13 from the *MLH3* gene locus, and the PCR product was used as template DNA for amplifying the 5′-arm. The 5′-arm was amplified using primers F14 and R14, where each primer shared 20-bp end homology with the insertion site of the vector. The sequence intended as the 3′-arm of the *MLH3*-targeting construct was amplified by PCR as two fragments using overlapping primers (F15 and R15 for $MLH3^{DN/DN}$ and F16 and R16 for $MLH3^{EK/EK}$ cells) that included a point mutation to change codon from aspartic acid to asparagine ($MLH3^{DN/DN}$) and glutamic acid to lysine ($MLH3^{EK/EK}$) subsequently. The two fragments were then combined by chimeric PCR to yield the 3′ targeting arm including the mutation. The 3′-arm was amplified using primers F17 and R17, where each primer shared 20-bp end homology with the insertion site of the vector. Both vectors, DT-ApA/neo and DT-ApA/hygro, were linearized with NotI and XbaI. All of the fragments of the vectors and inserts were purified using a QIAquick gel extraction kit (Qiagen). The gene-targeting constructs were generated in a single reaction mixture containing DT-ApA/neo or DT-ApA/hygro vectors, 5′- and 3′-arms, and 2× SLiCE buffer (Invitrogen) and incubated for 30 min at room temperature. 6 μg of CRISPR and 2 μg of each gene-targeting vector were transfected into 4×10^6 TK6 cells using the Neon Transfection System (Life Technologies). After electroporation, cells were released into 20 ml of drug-free medium containing 10% horse serum. 48 h later, cells were seeded into 96-well plates for selection with both neomycin and hygromycin antibiotics for 2 weeks. The site-directed mutagenesis was confirmed by genomic PCR using primers F18 and R18 followed by direct sequencing (Figs. S6, *C* and *D*). The drug resistance markers are flanked by *lox*P sites and were thus excised from $MLH3^{DN/DN}$ and $MLH3^{EK/EK}$ cells by transient expression of Cre recombinase, leading to the generation of $MLH3^{DN/DN}$ and $MLH3^{EK/EK}$ cells.

Colony survival assay

To measure sensitivity, cells were treated with camptothecin (Topogen, Inc.) and olaparib (Funakoshi, Tokyo, Japan) and irradiated with ionizing radiation (^{137}Cs). Cell sensitivity to these DNA-damaging agents was evaluated by counting colony formation in methylcellulose plates as described previously (87).

Heteroallelic crossover analysis

The human lymphoblastoid cell line TSCER2 is a TK6 derivative with an I-SceI site inserted into the TK locus (50, 51). TSCER2 cells are compound heterozygous ($TK^{-/-}$) for a point mutation in exons 4 and 5. A DSB occurring at the I-SceI site results in homologous recombination between the alleles and produces TK-proficient revertants ($TK^{+/-}$). 4×10^6 TK6 cells were transfected with 6 μg of I-SceI expression vector using the Neon Transfection System (Life Technologies) with 3× pulse at 1350 V and with 10-ms pulse width and released into 20 ml of drug-free medium containing 10% horse serum. After 48 h, cells were seeded as 1×10^6 cells/96-well plate, with 2′-deoxycytidine (Sigma, D0776), hypoxanthine (Sigma, H9377), aminopterin (Sigma, A3411), and thymidine (Sigma, T9250) (CHAT for TK-revertants) medium. Drug-resistant colonies were counted 2 weeks later.

Chromosomal aberration analysis

TK6 cells were irradiated with 1-Gy IR. The cells were then treated with 0.1 μg/ml colcemid (GIBCO-BRL) and incubated at 37 °C for 3 h. Experimental conditions for chromosomal aberration analysis were as described previously (72). Briefly, harvested cells were treated with 1 ml of 75 mM KCl for 15 min at room temperature and fixed in 5 ml of a freshly prepared 3:1 mixture of methanol/acetic acid. The cell suspension was dropped onto a glass slide and air-dried. The slides were stained with 5% Giemsa solution (Nacalai Tesque) for 10 min and air-dried after being rinsed carefully with water. All chromosomes in each mitotic cell were scored at ×1000 magnification. A total of 50 mitotic cells were scored for each group using a microscope.

SCE analysis

TK6 cells were incubated with or without cisplatin (2 μM). After 1 h, cells were washed and released into bromodeoxyuridine (100 mM)-containing media. Cells were incubated for two more cell cycles and treated with colcemid (0.1 mg/ml) for 3 h before being harvested. Metaphase chromosomes were prepared and assayed for SCEs as described previously (64).

Immunostaining and microscopic analysis

Cells were fixed with 4% paraformaldehyde (Nacalai Tesque) for 10 min at room temperature and permeabilized with 0.5% Triton X-100 (Sigma) for 30 min. Images were taken with a confocal microscope (TCS SP8, Leica Microsystems, Germany).

Antibodies

The following antibodies were used: anti-γH2AX mouse monoclonal (1:1000; Millipore); anti-Rad51 rabbit polyclonal (1:500; Sigma); anti-MLH1 (1:1000; ab92312, Abcam); anti-FLAG (1:500; F1804, Sigma); mouse monoclonal α-β-tubulin (Sigma); Alexa Fluor 488–conjugated anti-mouse IgG (1:1000; Molecular Probes); Alexa Fluor 488–conjugated anti-rabbit IgG (1:1000; Molecular Probes); and goat monoclonal α-mouse horseradish peroxidase (Invitrogen).

Construction of FLAG-tagged hGen1 with nuclear localization signal expressing TK6 cell lines

FLAG-tagged hGen1-NES (4A)-NLS^+-expressing TK6 cells were generated using a genetically modified retroviral vector as

described (Fig. S7) (72). Briefly, the coding sequence for hGen1-NES (4A)-3xNLS^{+}-3xFLAG was cloned into the pMSCV retroviral expression vector (Clontech) (Fig. S7*A*). The newly engineered retroviral expression vector was co-transfected into human 293T cells with a helper plasmid (pClampho) expressing the viral Gag, Pol, and Env proteins to produce viral supernatant. The viral supernatant was collected after 48 h and used to transduce into *WT*, *PMS2*$^{EK/EK}$, *MLH3*$^{DN/DN}$, *PMS2*$^{EK/EK}$/*MLH3*$^{DN/DN}$, *MUS81*$^{-/-}$, and *RAD54*$^{-/-}$ TK6 mutant strains (Fig. S7*B*). The efficiency of each step was assessed by quantifying the number of cells expressing GFP (Fig. S7*C*). The expression of hGen1-NES (4A)-3xNLS^{+}-3xFLAG was further confirmed by Western blotting. Experimental conditions for Western blotting analysis were as described previously (88). Anti-FLAG antibody overnight at 4 °C and anti-mouse IgG horseradish peroxidase–linked antibody for 1 h at room temperature were used as the primary and secondary antibodies, respectively (Fig. S7*D*).

Quantification and statistical analysis

For all statistical analyses with a p value, unpaired Student's t test was used. *Error bars* represent S.D., as indicated in the figure legends. We calculated the propagation of errors using the following formula: $\sqrt{((\text{S.D. with IR treatment})^2 + (\text{S.D. without IR treatment}))^2}$

Data availability

All of the data described are contained within the article.

Acknowledgments—We thank A. Noguchi, A. Kobayashi, and M. Kato for technical assistance and the laboratory members for stimulating discussions.

Author contributions—M. M. R., M. M., I. S. K., and S. T. conceptualization; H. S., J.-B. C., and S. T. resources; M. M. R., M. M., I. S. K., K. Y., M. T., H. S., J. A., and R. G. data curation; M. M. R., M. M., I. S. K., M. T., and H. S. formal analysis; H. S., J.-B. C., and S. T. supervision; H. S., J.-B. C., V. B., and S. T. funding acquisition; M. M. R., M. M., I. S. K., J.-B. C., and S. T. methodology; M. M. R., M. M., I. S. K., J.-B. C., and S. T. writing-original draft; M. M. R., M. M., and S. T. project administration; J. A. and R. G. software; V. B. and J.-B. C. writing-review and editing.

Funding and additional information—This work was directly supported by grants-in-aid from the Ministry of Education, Science, Sport, and Culture (KAKENHI 25650006, 23221005, 19K22561, and 16H06306 (to S. T.) and KAKENHI 16H02953, 18H04900, and 19H04267 (to H. S.)), Agence Nationale de la Recherche (ANR) Grant ANR-15-CE11-0011 (to V. B. and J.-B. C.), and by French Infrastructure for Integrated Structural Biology (FRISBI) Grant ANR-10-INBS-05 (to J.-B. C.). This work was also supported by the Japan Society for the Promotion of Science Core-to-Core Program, Advanced Research Networks (to S. T.). This study was conducted through the Joint Research Program of the Radiation Biology Center, Kyoto.

Conflict of interest—The authors declare that they have no conflicts of interest with the contents of this article.

Abbreviations—The abbreviations used are: MMR, mismatch repair; DSB, double-strand break; NHEJ, nonhomologous end-joining; HR, homologous recombination; JM, joint molecule; HJ, Holliday junction; dHJ, double Holliday junction; SCE, sister chromatid exchange; NES, nuclear export signal; NLS, nuclear localization signal; SLiCE, seamless ligation cloning extract; TK, thymidine kinase; Gy, gray; PARP, poly(ADP-ribose) polymerase.

References

1. Iyer, R. R., Pluciennik, A., Burdett, V., and Modrich, P. L. (2006) DNA mismatch repair: functions and mechanisms. *Chem. Rev.* **106,** 302–323 CrossRef Medline
2. Jiricny, J. (2006) The multifaceted mismatch-repair system. *Nat. Rev. Mol. Cell Biol.* **7,** 335–346 CrossRef Medline
3. Hoffmann, E. R., and Borts, R. H. (2004) Meiotic recombination intermediates and mismatch repair proteins. *Cytogenet. Genome Res.* **107,** 232–248 CrossRef Medline
4. Modrich, P., and Lahue, R. (1996) Mismatch repair in replication fidelity, genetic recombination, and cancer biology. *Annu. Rev. Biochem.* **65,** 101–133 CrossRef Medline
5. Kunkel, T. A., and Erie, D. A. (2015) Eukaryotic mismatch repair in relation to DNA replication. *Annu. Rev. Genet.* **49,** 291–313 CrossRef Medline
6. Harfe, B. D., and Jinks-Robertson, S. (2000) DNA mismatch repair and genetic instability. *Annu. Rev. Genet.* **34,** 359–399 CrossRef Medline
7. Kolodner, R. D., and Marsischky, G. T. (1999) Eukaryotic DNA mismatch repair. *Curr. Opin. Genet. Dev.* **9,** 89–96 CrossRef
8. Marsischky, G. T., Filosi, N., Kane, M. F., and Kolodner, R. (1996) Redundancy of *Saccharomyces cerevisiae* MSH3 and MSH6 in MSH2-dependent mismatch repair. *Genes Dev.* **10,** 407–420 CrossRef Medline
9. Sia, E. A., Kokoska, R. J., Dominska, M., Greenwell, P., and Petes, T. D. (1997) Microsatellite instability in yeast: dependence on repeat unit size and DNA mismatch repair genes. *Mol. Cell. Biol.* **17,** 2851–2858 CrossRef Medline
10. Srivatsan, A., Bowen, N., and Kolodner, R. D. (2014) Mispair-specific recruitment of the Mlh1-Pms1 complex identifies repair substrates of the *Saccharomyces cerevisiae* Msh2-Msh3 complex. *J. Biol. Chem.* **289,** 9352–9364 CrossRef Medline
11. Goellner, E. M., Putnam, C. D., and Kolodner, R. D. (2015) Exonuclease 1-dependent and independent mismatch repair. *DNA Repair (Amst.)* **32,** 24–32 CrossRef Medline
12. Flores-Rozas, H., and Kolodner, R. D. (1998) The *Saccharomyces cerevisiae* MLH3 gene functions in MSH3-dependent suppression of frameshift mutations. *Proc. Natl. Acad. Sci. U. S. A.* **95,** 12404–12409 CrossRef Medline
13. Matton, N., 1,Simonetti, J., and W, K. (2000) Identification of mismatch repair protein complexes in HeLa nuclear extracts and their interaction with heteroduplex DNA. *J. Biol. Chem.* **275,** 17808–17813 CrossRef Medline
14. Gueneau, E., Dherin, C., Legrand, P., Tellier-Lebegue, C., Gilquin, B., Bonnesoeur, P., Londino, F., Quemener, C., Le Du, M.-H., Márquez, J. A., Moutiez, M., Gondry, M., Boiteux, S., and Charbonnier, J.-B. (2013) Structure of the MutLα C-terminal domain reveals how Mlh1 contributes to Pms1 endonuclease site. *Nat. Struct. Mol. Biol.* **20,** 461–468 CrossRef Medline
15. Kadyrov, F. A., Dzantiev, L., Constantin, N., and Modrich, P. (2006) Endonucleolytic function of MutLα in human mismatch repair. *Cell* **126,** 297–308 CrossRef Medline
16. de Wind, N., Dekker, M., Berns, A., Radman, M., and Te Riele, H. (1995) Inactivation of the mouse Msh2 gene results in mismatch repair deficiency, methylation tolerance, hyperrecombination, and predisposition to cancer. *Cell* **82,** 321–330 CrossRef Medline

17. Elliott, B., and Jasin, M. (2001) Repair of double-strand breaks by homologous recombination in mismatch repair-defective mammalian cells. *Mol. Cell Biol.* **21,** 2671–2682 CrossRef Medline
18. Sharma, S., Doherty, K. M., and Brosh, R. M. (2006) Mechanisms of RecQ helicases in pathways of DNA metabolism and maintenance of genomic stability. *Biochem. J.* **398,** 319–337 CrossRef Medline
19. Bannister, L. A., Waldman, B. C., and Waldman, A. S. (2004) Modulation of error-prone double-strand break repair in mammalian chromosomes by DNA mismatch repair protein Mlh1. *DNA Repair (Amst.)* **3,** 465–474 CrossRef Medline
20. Shibata, A., Conrad, S., Birraux, J., Geuting, V., Barton, O., Ismail, A., Kakarougkas, A., Meek, K., Taucher-Scholz, G., Löbrich, M., and Jeggo, P. A. (2011) Factors determining DNA double-strand break repair pathway choice in G_2 phase. *EMBO J.* **30,** 1079–1092 CrossRef Medline
21. Zakharyevich, K., Tang, S., Ma, Y., and Hunter, N. (2012) Delineation of joint molecule resolution pathways in meiosis identifies a crossover-specific resolvase. *Cell* **149,** 334–347 CrossRef Medline
22. Toledo, M., Sun, X., Brieño-Enríquez, M. A., Raghavan, V., Gray, S., Pea, J., Milano, C. R., Venkatesh, A., Patel, L., Borst, P. L., Alani, E., and Cohen, P. E. (2019) A mutation in the endonuclease domain of mouse MLH3 reveals novel roles for mutlγ during crossover formation in meiotic prophase I. *PLoS Genet.* **15,** e1008177 CrossRef Medline
23. Baker, S. M., Bronner, C. E., Zhang, L., Plug, A. W., Robatzek, M., Warren, G., Elliott, E. A., Yu, J., Ashley, T., Arnheim, N., Flavell, R. A., and Liskay, R. M. (1995) Male mice defective in the DNA mismatch repair gene PMS2 exhibit abnormal chromosome synapsis in meiosis. *Cell* **82,** 309–319 CrossRef Medline
24. Baker, S. M., Plug, A. W., Prolla, T. A., Bronner, C. E., Harris, A. C., Yao, X., Christie, D. M., Monell, C., Arnheim, N., Bradley, A., Ashley, T., and Liskay, R. M. (1996) Involvement of mouse Mlh1 in DNA mismatch repair and meiotic crossing over. *Nat. Genet.* **13,** 336–342 CrossRef Medline
25. Edelmann, W., Cohen, P. E., Kane, M., Lau, K., Morrow, B., Bennett, S., Umar, A., Kunkel, T., Cattoretti, G., Chaganti, R., Pollard, J. W., Kolodner, R. D., and Kucherlapati, R. (1996) Meiotic pachytene arrest in MLH1-deficient mice. *Cell* **85,** 1125–1134 CrossRef Medline
26. Lipkin, S. M., Moens, P. B., Wang, V., Lenzi, M., Shanmugarajah, D., Gilgeous, A., Thomas, J., Cheng, J., Touchman, J. W., Green, E. D., Schwartzberg, P., Collins, F. S., and Cohen, P. E. (2002) Meiotic arrest and aneuploidy in MLH3-deficient mice. *Nat. Genet.* **31,** 385–390 CrossRef Medline
27. Svetlanov, A., Baudat, F., Cohen, P. E., and De Massy, B. (2008) Distinct functions of MLH3 at recombination hot spots in the mouse. *Genetics* **178,** 1937–1945 CrossRef Medline
28. Fischer, J. M., Dudley, S., Miller, A. J., and Liskay, R. M. (2016) An intact Pms2 ATPase domain is not essential for male fertility. *DNA Repair* **39,** 46–51 CrossRef Medline
29. Cannavo, E., Sanchez, A., Anand, R., Ranjha, L., Hugener, J., Adam, C., Acharya, A., Weyland, N., Aran-Guiu, X., Charbonnier, J.-B., Hoffmann, E. R., Borde, V., Matos, J., and Cejka, P. (2020) Regulation of the MLH1–MLH3 endonuclease in meiosis. *Nature* **586,** 618–622 CrossRef Medline
30. Kulkarni, D., Owens, S., Honda, M., Ito, M., Yang, Y., Corrigan, M., Chen, L., Quan, A., and Hunter, N. (2020) PCNA activates the MutLγ endonuclease to promote meiotic crossing over. *Nature* **586,** 623–627 CrossRef Medline
31. Takeda, S., Nakamura, K., Taniguchi, Y., and Paull, T. T. (2007) Ctp1/CtIP and the MRN complex collaborate in the initial steps of homologous recombination. *Mol. Cell* **28,** 351–352 CrossRef Medline
32. Bernstein, K. A., and Rothstein, R. (2009) At loose ends: resecting a double-strand break. *Cell* **137,** 807–810 CrossRef Medline
33. Mehta, A., and Haber, J. E. (2014) Sources of DNA double-strand breaks and models of recombinational DNA repair. *Cold Spring Harb. Perspect. Biol.* **6,** a016428 CrossRef Medline
34. Sugawara, N., Wang, X., and Haber, J. E. (2003) *In vivo* roles of Rad52, Rad54, and Rad55 proteins in Rad51-mediated recombination. *Mol. Cell* **12,** 209–219 CrossRef Medline
35. Dion, V., Kalck, V., Horigome, C., Towbin, B. D., and Gasser, S. M. (2012) Increased mobility of double-strand breaks requires Mec1, Rad9 and the homologous recombination machinery. *Nat. Cell Biol.* **14,** 502–509 CrossRef Medline
36. Schwartz, E. K., and Heyer, W. D. (2011) Processing of joint molecule intermediates by structure-selective endonucleases during homologous recombination in eukaryotes. *Chromosoma* **120,** 109–127 CrossRef Medline
37. West, S. C., Blanco, M. G., Chan, Y. W., Matos, J., Sarbajna, S., and Wyatt, H. D. M. (2015) Resolution of recombination intermediates: mechanisms and regulation. *Cold Spring Harbor Symp. Quant. Biol.* **80,** 103–109 CrossRef Medline
38. Wyatt, H. D. M., Laister, R. C., Martin, S. R., Arrowsmith, C. H., and West, S. C. (2017) The SMX DNA repair tri-nuclease. *Mol. Cell* **65,** 848–860.e11 CrossRef Medline
39. Kikuchi, K., Narita, T., Pham, V. T., Iijima, J., Hirota, K., Keka, I. S., Mohiuddin, Okawa, K., Hori, T., Fukagawa, T., Essers, J., Kanaar, R., Whitby, M. C., Sugasawa, K., Taniguchi, Y., Kitagawa, K., *et al.* (2013) Structure-specific endonucleases Xpf and Mus81 play overlapping but essential roles in DNA repair by homologous recombination. *Cancer Res.* **73,** 4362–4371 CrossRef Medline
40. Abraham, J., Lemmers, B., Hande, M. P., Moynahan, M. E., Chahwan, C., Ciccia, A., Essers, J., Hanada, K., Chahwan, R., Khaw, A. K., McPherson, P., Shehabeldin, A., Laister, R., Arrowsmith, C., Kanaar, R., *et al.* (2003) Eme1 is involved in DNA damage processing and maintenance of genomic stability in mammalian cells. *EMBO J.* **22,** 6137–6147 CrossRef Medline
41. McPherson, J. P., Lemmers, B., Chahwan, R., Pamidi, A., Migon, E., Matysiak-Zablocki, E., Moynahan, M. E., Essers, J., Hanada, K., Poonepalli, A., Sanchez-Sweatman, O., Khokha, R., Kanaar, R., Jasin, M., Hande, M. P., *et al.* (2004) Involvement of mammalian Mus81 in genome integrity and tumor suppression. *Science* **304,** 1822–1826 CrossRef Medline
42. Castor, D., Nair, N., Déclais, A. C., Lachaud, C., Toth, R., Macartney, T. J., Lilley, D. M. J., Arthur, J. S. C., and Rouse, J. (2013) Cooperative control of Holliday junction resolution and DNA repair by the SLX1 and MUS81-EME1 nucleases. *Mol. Cell* **52,** 221–233 CrossRef Medline
43. Wang, X., Wang, H., Guo, B., Zhang, Y., Gong, Y., Zhang, C., Xu, H., and Wu, X. (2016) Gen1 and Eme1 Play Redundant Roles in DNA Repair and Meiotic Recombination in Mice. *DNA Cell Biol.* **35,** 585–590 CrossRef Medline
44. Kaur, H., De Muyt, A., and Lichten, M. (2015) Top3-Rmi1 DNA single-strand decatenase is integral to the formation and resolution of meiotic recombination intermediates. *Mol. Cell* **57,** 583–594 CrossRef Medline
45. Tang, S., Wu, M. K. Y., Zhang, R., and Hunter, N. (2015) Pervasive and essential roles of the Top3-Rmi1 decatenase orchestrate recombination and facilitate chromosome segregation in meiosis. *Mol. Cell* **57,** 607–621 CrossRef Medline
46. Takata, M., Sasaki, M. S., Sonoda, E., Morrison, C., Hashimoto, M., Utsumi, H., Yamaguchi-Iwai, Y., Shinohara, A., and Takeda, S. (1998) Homologous recombination and non-homologous end-joining pathways of DNA double-strand break repair have overlapping roles in the maintenance of chromosomal integrity in vertebrate cells. *EMBO J.* **17,** 5497–5508 CrossRef Medline
47. Keka, I. S., Mohiuddin, Maede, Y., Rahman, M. M., Sakuma, T., Honma, M., Yamamoto, T., Takeda, S., and Sasanuma, H. (2015) Smarcal1 promotes double-strand-break repair by nonhomologous end-joining. *Nucleic Acids Res.* **43,** 6359–6372 CrossRef Medline
48. Murai, J., Huang, S. Y. N., Das, B. B., Renaud, A., Zhang, Y., Doroshow, J. H., Ji, J., Takeda, S., and Pommier, Y. (2012) Trapping of PARP1 and PARP2 by clinical PARP inhibitors. *Cancer Res.* **72,** 5588–5599 CrossRef Medline
49. Fowler, P., Whitwell, J., Jeffrey, L., Young, J., Smith, K., and Kirkland, D. (2010) Cadmium chloride, benzo[a]pyrene and cyclophosphamide tested in the *in vitro* mammalian cell micronucleus test (MNvit) in the human lymphoblastoid cell line TK6 at Covance laboratories, Harrogate UK in support of OECD draft Test Guideline 487. *Mutat. Res.* **702,** 171–174 CrossRef Medline
50. Honma, M., Izumi, M., Sakuraba, M., Tadokoro, S., Sakamoto, H., Wang, W., Yatagai, F., and Hayashi, M. (2003) Deletion, rearrangement, and gene conversion; genetic consequences of chromosomal double-strand breaks in human cells. *Environ. Mol. Mutagen.* **42,** 288–298 CrossRef Medline

51. Neuwirth, E. A H., Honma, M., and Grosovsky, A. J. (2007) Interchromosomal crossover in human cells is associated with long gene conversion tracts. *Mol. Cell. Biol.* **27,** 5261–5274 CrossRef Medline
52. Yoshimoto, K., Mizoguchi, M., Hata, N., Murata, H., Hatae, R., Amano, T., Nakamizo, A., and Sasaki, T. (2012) Complex DNA repair pathways as possible therapeutic targets to overcome temozolomide resistance in glioblastoma. *Front. Oncol.* **2,** 186 CrossRef Medline
53. Cejka, P., Stojic, L., Mojas, N., Russell, A. M., Heinimann, K., Cannavó, E., Di Pietro, M., Marra, G., and Jiricny, J. (2003) Methylation-induced G_2/M arrest requires a full complement of the mismatch repair protein hMLH1. *EMBO J.* **22,** 2245–2254 CrossRef Medline
54. Kadyrov, F. A., Holmes, S. F., Arana, M. E., Lukianova, O. A., O'Donnell, M., Kunkel, T. A., and Modrich, P. (2007) *Saccharomyces cerevisiae* MutLα is a mismatch repair endonuclease. *J. Biol. Chem.* **282,** 37181–37190 CrossRef Medline
55. Deschênes, S. M., Tomer, G., Nguyen, M., Erdeniz, N., Juba, N. C., Sepúlveda, N., Pisani, J. E., and Liskay, R. M. (2007) The E705K mutation in hPMS2 exerts recessive, not dominant, effects on mismatch repair. *Cancer Lett.* **249,** 148–156 CrossRef Medline
56. Nishant, K. T., Plys, A. J., and Alani, E. (2008) A mutation in the putative MLH3 endonuclease domain confers a defect in both mismatch repair and meiosis in *Saccharomyces cerevisiae*. *Genetics* **179,** 747–755 CrossRef Medline
57. Kadyrova, L. Y., Gujar, V., Burdett, V., Modrich, P. L., and Kadyrov, F. A. (2020) Human MutLγ, the MLH1–MLH3 heterodimer, is an endonuclease that promotes DNA expansion. *Proc. Natl. Acad. Sci. U. S. A.* **117,** 3535–3542 CrossRef Medline
58. Al-Sweel, N., Raghavan, V., Dutta, A., Ajith, V. P., Di Vietro, L., Khondakar, N., Manhart, C. M., Surtees, J. A., Nishant, K. T., and Alani, E. (2017) Mlh3 mutations in baker's yeast alter meiotic recombination outcomes by increasing noncrossover events genome-wide. *PLoS Genet.* **13,** e1007067 CrossRef Medline
59. Shimizu, N., Akagawa, R., Takeda, S., and Sasanuma, H. (2020) The MRE11 nuclease promotes homologous recombination not only in DNA double-strand break resection but also in post-resection in human TK6 cells. *Genome Instability Dis.* **1,** 184–196 CrossRef
60. Hoa, N. N., Akagawa, R., Yamasaki, T., Hirota, K., Sasa, K., Natsume, T., Kobayashi, J., Sakuma, T., Yamamoto, T., Komatsu, K., Kanemaki, M. T., Pommier, Y., Takeda, S., and Sasanuma, H. (2015) Relative contribution of four nucleases, CtIP, Dna2, Exo1 and Mre11, to the initial step of DNA double-strand break repair by homologous recombination in both the chicken DT40 and human TK6 cell lines. *Genes Cells* **20,** 1059–1076 CrossRef Medline
61. Fujita, M., Sasanuma, H., Yamamoto, K. N., Harada, H., Kurosawa, A., Adachi, N., Omura, M., Hiraoka, M., Takeda, S., and Hirota, K. (2013) Interference in DNA replication can cause mitotic chromosomal breakage unassociated with double-strand breaks. *PLoS ONE* **8,** e60043 CrossRef Medline
62. Wechsler, T., Newman, S., and West, S. C. (2011) Aberrant chromosome morphology in human cells defective for Holliday junction resolution. *Nature* **471,** 642–646 CrossRef Medline
63. Suzuki, T., Yasui, M., and Honma, M. (2016) Mutator phenotype and DNA double-strand break repair in BLM helicase-deficient human cells. *Mol. Cell Biol.* **36,** 2877–2889 CrossRef Medline
64. Sonoda, E., Sasaki, M. S., Morrison, C., Yamaguchi-Iwai, Y., Takata, M., and Takeda, S. (1999) Sister chromatid exchanges are mediated by homologous recombination in vertebrate cells. *Mol. Cell. Biol.* **19,** 5166–5169 CrossRef Medline
65. Wyatt, H. D. M., Sarbajna, S., Matos, J., and West, S. C. (2013) Coordinated actions of SLX1-SLX4 and MUS81-EME1 for holliday junction resolution in human cells. *Mol. Cell* **52,** 234–247 CrossRef Medline
66. Jiricny, J. (2013) Postreplicative mismatch repair. *Cold Spring Harb. Perspect. Biol.* **5,** a012633 CrossRef Medline
67. Söding, J., Biegert, A., and Lupas, A. N. (2005) The HHpred interactive server for protein homology detection and structure prediction. *Nucleic Acids Res.* **33,** W244–W248 CrossRef
68. Zimmermann, L., Stephens, A., Nam, S. Z., Rau, D., Kübler, J., Lozajic, M., Gabler, F., Söding, J., Lupas, A. N., and Alva, V. (2018) A completely reimplemented MPI bioinformatics toolkit with a new HHpred server at its core. *J. Mol. Biol.* **430,** 2237–2243 CrossRef Medline
69. Song, Y., Dimaio, F., Wang, R. Y. R., Kim, D., Miles, C., Brunette, T., Thompson, J., and Baker, D. (2013) High-resolution comparative modeling with RosettaCM. *Structure* **21,** 1735–1742 CrossRef Medline
70. Lorenz, A., West, S. C., and Whitby, M. C. (2010) The human Holliday junction resolvase GEN1 rescues the meiotic phenotype of a *Schizosaccharomyces pombe* mus81 mutant. *Nucleic Acids Res.* **38,** 1866–1873 CrossRef Medline
71. Chan, Y. W., and West, S. C. (2014) Spatial control of the GEN1 Holliday junction resolvase ensures genome stability. *Nat. Commun.* **5,** 4844 CrossRef Medline
72. Mohiuddin, Keka, I. S., Evans, T. J., Hirota, K., Shimizu, H., Kono, K., Takeda, S., and Hirano, S. (2014) A novel genotoxicity assay of carbon nanotubes using functional macrophage receptor with collagenous structure (MARCO)-expressing chicken B lymphocytes. *Arch. Toxicol.* **88,** 145–160 CrossRef Medline
73. Zeng, M., Narayanan, L., Xu, X. S., Prolla, T. A., Liskay, R. M., and Glazer, P. M. (2000) Ionizing radiation-induced apoptosis via separate Pms2- and p53-dependent pathways. *Cancer Res.* **60,** 4889–4893 Medline Medline
74. Shcherbakova, P. V., Hall, M. C., Lewis, M. S., Bennett, S. E., Martin, K. J., Bushel, P. R., Afshari, C. A., and Kunkel, T. A. (2001) Inactivation of DNA mismatch repair by increased expression of yeast MLH1. *Mol. Cell. Biol.* **21,** 940–951 CrossRef Medline
75. Sanchez, A., Adam, C., Rauh, F., Duroc, Y., Ranjha, L., Lombard, B., Mu, X., Loew, D., Keeney, S., Cejka, P., Guérois, R., Klein, F., Charbonnier, J.-B., and Borde, V. (2020) Mechanism of *in vivo* activation of the MutLγ-Exo1 complex for meiotic crossover formation. *bioRxiv* 10.1101/2019.12.16.876623 CrossRef
76. Chen, P. C., Dudley, S., Hagen, W., Dizon, D., Paxton, L., Reichow, D., Yoon, S. R., Yang, K., Arnheim, N., Liskay, R. M., and Lipkin, S. M. (2005) Contributions by MutL homologues Mlh3 and Pms2 to DNA mismatch repair and tumor suppression in the mouse. *Cancer Res.* **65,** 8662–8670 CrossRef Medline
77. Sarbajna, S., Davies, D., and West, S. C. (2014) Roles of SLX1-SLX4, MUS81-EME1, and GEN1 in avoiding genome instability and mitotic catastrophe. *Genes Dev.* **28,** 1124–1136 CrossRef Medline
78. Garner, E., Kim, Y., Lach, F. P., Kottemann, M. C., and Smogorzewska, A. (2013) Human GEN1 and the SLX4-associated nucleases MUS81 and SLX1 are essential for the resolution of replication-induced Holliday junctions. *Cell Rep.* **5,** 207–215 CrossRef Medline
79. West, S. C., and Chan, Y. W. (2017) Genome instability as a consequence of defects in the resolution of recombination intermediates. *Cold Spring Harb. Symp. Quant. Biol.* **82,** 207–212 CrossRef Medline
80. Hodskinson, M. R. G., Silhan, J., Crossan, G. P., Garaycoechea, J. I., Mukherjee, S., Johnson, C. M., Schärer, O. D., and Patel, K. J. (2014) Mouse SLX4 is a tumor suppressor that stimulates the activity of the nuclease XPF-ERCC1 in DNA crosslink repair. *Mol. Cell.* **54,** 472–484 CrossRef Medline
81. Pamidi, A., Cardoso, R., Hakem, A., Matysiak-Zablocki, E., Poonepalli, A., Tamblyn, L., Perez-Ordonez, B., Hande, M. P., Sanchez, O., and Hakem, R. (2007) Functional interplay of p53 and Mus81 in DNA damage responses and cancer. *Cancer Res.* **67,** 8527–8535 CrossRef Medline
82. Wang, T. F., Kleckner, N., and Hunter, N. (1999) Functional specificity of MutL homologs in yeast: evidence for three Mlh1-based heterocomplexes with distinct roles during meiosis in recombination and mismatch correction. *Proc. Natl. Acad. Sci. U. S. A.* **96,** 13914–13919 CrossRef Medline
83. Mohiuddin, M., Evans, T. J., Rahman, M. M., Keka, I. S., Tsuda, M., Sasanuma, H., and Takeda, S. (2018) SUMOylation of PCNA by PIAS1 and PIAS4 promotes template switch in the chicken and human B cell lines. *Proc. Natl. Acad. Sci. U. S. A.* **115,** 12793–12798 CrossRef Medline
84. Cermak, T., Doyle, E. L., Christian, M., Wang, L., Zhang, Y., Schmidt, C., Baller, J. A., Somia, N. V., Bogdanove, A. J., Voytas, D. F. (2011) Efficient design and assembly of custom TALEN and other TAL effector-based constructs for DNA targeting. *Nucleic Acids* **39,** e82 CrossRef Medline
85. Sakuma, T., Ochiai, H., Kaneko, T., Mashimo, T., Tokumasu, D., Sakane, Y., Suzuki, K., Miyamoto, T., Sakamoto, N., Matsuura, S., and Yamamoto, T. (2013) Repeating pattern of non-RVD variations in

DNA-binding modules enhances TALEN activity. *Sci. Rep.* **3,** 3379 CrossRef Medline

86. Ran, F. A., Hsu, P. D., Lin, C. Y., Gootenberg, J. S., Konermann, S., Trevino, A. E., Scott, D. A., Inoue, A., Matoba, S., Zhang, Y., and Zhang, F. (2013) Double nicking by RNA-guided CRISPR cas9 for enhanced genome editing specificity. *Cell* **154,** 1380–1389 CrossRef Medline
87. Mohiuddin, M., Rahman, M. M., Sale, J. E., and Pearson, C. E. (2019) CtIP-BRCA1 complex and MRE11 maintain replication forks in the presence of chain terminating nucleoside analogs. *Nucleic Acids Res.* **47,** 2966–2980 CrossRef Medline
88. Mohiuddin, Kobayashi, , S., Keka, I. S., Guilbaud, G., Sale, J., Narita, T., Abdel-Aziz, H. I., Wang, X., Ogawa, S., Sasanuma, H., Chiu, R., Oestergaard, V. H., and Lisby, M. T. S. (2016) The role of HERC2 and RNF8 ubiquitin E3 ligases in the promotion of translesion DNA synthesis in the chicken DT40 cell line. *DNA Repair (Amst.)* **40,** 67–76 CrossRef Medline